



## Role for RIF1-interacting partner DDX1 in BLM recruitment to DNA double-strand breaks

Lei Li<sup>a</sup>, Ho-Yin Poon<sup>a</sup>, Matthew R. Hildebrandt<sup>a</sup>, Elizabeth A. Monckton<sup>a</sup>, Devon R. Germain<sup>a</sup>, Richard P. Fahlman<sup>b</sup>, Roseline Godbout<sup>a,\*</sup>

<sup>a</sup> Department of Oncology, Cross Cancer Institute, University of Alberta, 11560 University Avenue, Edmonton Alberta T6G 1Z2, Canada

<sup>b</sup> Department of Biochemistry, University of Alberta Edmonton Alberta, Canada

### ARTICLE INFO

#### Keywords:

DNA double strand break repair  
RNA helicase  
Homologous recombination  
Non-homologous end joining  
Protein-protein interaction

### ABSTRACT

Human Rap1-interacting factor 1 (RIF1) is an important player in the repair of DNA double strand breaks (DSBs). RIF1 acts downstream of 53BP1, with well-documented roles in class switch recombination in B-cells and inhibition of end resection initiation in BRCA1-defective cells. Here, we report that DEAD Box 1 (DDX1), a RNA helicase also implicated in DSB repair, interacts with RIF1, with co-localization of DDX1 and RIF1 observed throughout interphase. Recruitment of DDX1 to DSBs is dependent on RIF1, with RIF1 depletion abolishing DDX1-mediated facilitation of homologous recombination at DSBs. As previously demonstrated for RIF1, DDX1 is also required for chromatin loading of Bloom syndrome helicase (BLM) to ionizing radiation-induced DSBs, a RIF1-related activity that is independent of 53BP1. We show that DDX1 and RIF1 have different nucleic acid requirements for accumulation at DSBs, with RNA-DNA hybrids required for DDX1 accrual at DSBs, and single-strand RNA required for accumulation of RIF1 at these sites. Our data suggest both convergent and divergent roles for DDX1 and RIF1 in DSB repair, and may help explain why RIF1 depletion does not fully mimic 53BP1 ablation in the restoration of homologous recombination defects in BRCA1-deficient cells.

### 1. Introduction

Cells are continuously subjected to DNA damage, which generates thousands of DNA lesions per cell each day [1]. DNA double strand breaks (DSBs) are the most harmful DNA lesions, as failure to repair DSBs can lead to genomic instability and cancer. DSBs are primarily repaired by error-free homologous recombination (HR) with intact homologous DNA sequences serving as the repair template, and error-prone non-homologous end joining (NHEJ) whereby the two broken DNA ends are ligated together often resulting in loss of genetic information [2,3]. Deficiencies in one of these repair pathways often lead to compensation by the other pathway, suggesting crosstalk between HR and NHEJ repair proteins, with the best known examples being tumor suppressors Breast Cancer 1 (BRCA1) and p53-binding protein 1 (53BP1) [2,3]. While inactivation of BRCA1 results in defective HR, chromosomal abnormalities and tumorigenesis, all of these defects can be corrected by 53BP1 inactivation [4,5]. In turn, 53BP1 suppresses HR via two downstream effectors: Rap1-interacting factor 1 (RIF1) and Pax transactivation domain-interacting protein

(PTIP) [6–11]. As none of these three proteins appear to have enzymatic activity in DSB repair [6,12–14], they are believed to act as scaffolds that recruit additional effectors with enzymatic activities to carry out DSB repair.

There is increasing evidence supporting a role for RNA metabolism proteins in cellular response to DSBs [15–17]. We previously reported that DEAD Box 1 (DDX1) is recruited to a subset of DSBs in cells exposed to ionizing radiation (IR), with retention at DSBs dependent on the presence of RNA-DNA hybrids and active transcription [18,19]. DDX1 promotes cell survival post IR and facilitates HR-mediated DSB repair by protecting the single-stranded DNA once it is generated by end resection [19]. Ataxia-telangiectasia mutated (ATM)-dependent phosphorylation of DDX1 is required for DDX1 recruitment at DSBs, a post-translational modification that has been associated with the maturation of DSB-induced microRNAs [18,20].

DDX1 is overexpressed in a subset of retinoblastoma and neuroblastoma cancers and cell lines [20–23]. In breast cancer, elevated levels of DDX1 are associated with poor prognosis [23]. DDX1 is ubiquitously expressed and essential for early embryonic development

*Abbreviations:* BLM, Bloom syndrome helicase; DDX1, DEAD Box 1; DSB, double strand break; Gy, gray; HR, homologous recombination; IR, ionizing radiation; NHEJ, non-homologous end joining; RIF1, Rap1-interacting factor 1; RNase, ribonuclease

\* Corresponding author.

E-mail address: [rgodbout@ualberta.ca](mailto:rgodbout@ualberta.ca) (R. Godbout).

<http://dx.doi.org/10.1016/j.dnarep.2017.05.001>

Received 1 February 2017; Received in revised form 1 May 2017; Accepted 2 May 2017

Available online 13 May 2017

1568-7864/ © 2017 Elsevier B.V. All rights reserved.

in mouse [24]. In flies, disruption of *DDX1* leads to reduced size and infertility [25]. Functional studies have revealed roles for *DDX1* in RNA transport granules in neurons [26,27], cellular response to virus infection [28–30] and biogenesis of tRNAs [31].

To gain further insight into the role of *DDX1* in the DSB response, we used co-immunoprecipitation followed by mass spectrometry to identify interacting partners of *DDX1*. *RIF1*, the downstream effector of 53BP1, was identified as a *DDX1* interacting partner in both the presence and absence of DNA damage. Our data indicate that *RIF1* is required for *DDX1* recruitment to DSBs, as well as for *DDX1*-dependent facilitation of DSB repair by HR. Furthermore, *DDX1* depletion significantly impairs *RIF1*-dependent chromatin loading of BLM to DNA damage sites, a 53BP1-independent activity previously associated with *RIF1* [10]. We propose a model whereby *RIF1* plays different roles in DSB repair depending on its interacting partners.

## 2. Materials and methods

### 2.1. Cell culture and $\gamma$ -irradiation

HeLa, U2OS, HEK293, U2OS DR-GFP and U2OS EJ5-GFP cells were cultured in DMEM (Invitrogen) supplemented with 10% fetal calf serum (FCS), 100 U/ml penicillin and 100  $\mu$ g/ml streptomycin. BT (ATM-positive, normal) and L3 (ATM-negative, A-T patient) lymphoblastoid cell lines were cultured in RPMI 1640 (Invitrogen) supplemented with FCS and antibiotics as described above. Cells were  $\gamma$ -irradiated using a Shepherd <sup>137</sup>Cs irradiator (San Fernando, CA) and allowed to recover at 37 °C for the indicated times prior to analysis.

### 2.2. Mass spectrometry and co-immunoprecipitation

HeLa whole cell lysates were prepared by resuspending the cells in lysis buffer [50 mM Tris-HCl pH 7.5, 150 mM NaCl, 0.5% sodium deoxycholate, 1% NP-40, and 1X Complete protease inhibitors (Roche)]. Cell lysates were passed through 23 gauge needles to extract proteins bound to the nuclear matrix. Co-immunoprecipitations were carried out in lysis buffer with 0.1% sodium deoxycholate and 0.2% NP-40. Approximately 1 mg of lysate was incubated with either 5  $\mu$ l rabbit anti-*DDX1* antibody (batch 2910) or rabbit pre-immune serum. Immunoprecipitates were washed three times in lysis buffer. A total of five immunoprecipitations (from a total of 5 mg lysate) were pooled and electrophoresed in a 10% acrylamide SDS gel followed by colloidal Coomassie Blue G-250 staining [32]. Protein bands that were present in the *DDX1* immunoprecipitation lane but absent in the pre-immune lane were sliced from the gel. Protein bands were then subjected to reduction and alkylation followed by in-gel trypsin digestion. The digested peptides were analyzed by nano-LC-MS/MS and the raw data submitted to the MASCOT server for error tolerant protein identification [33]. The LC separation was performed on an Agilent 1100/1200 nano HPLC using a 10% A to 60% B gradient over 40 mins (A: 0.2% formic acid; B: 95% methanol, 0.2% formic acid). MS analysis was performed using an LCQ Deca Ion Trap mass spectrometer (Thermo Fisher Scientific). Co-immunoprecipitations were also carried out using a different anti-*DDX1* antibody (batch 2923).

To confirm the mass spectrometry results, co-immunoprecipitations were carried out using 500  $\mu$ g HeLa whole cell lysates and 4  $\mu$ l anti-*DDX1* antibody. Immunoprecipitates were resolved in an 8% acrylamide low-Bis SDS gel followed by transfer to nitrocellulose membranes. Blots were immunostained with rabbit anti-*RIF1* antibody (1:100; Novus Biologicals). Reciprocal co-immunoprecipitations were carried out using rabbit anti-*RIF1* antibody [gift from Dr. Weidong Wang (NIA, NIH)] followed by immunoblotting with anti-*DDX1* antibody. Reciprocal co-IPs were also performed using rabbit anti-*BLM* antibody (Bethyl Laboratories) followed by immunoblotting with anti-*DDX1* antibody. Where indicated, 500  $\mu$ g HeLa lysates were incubated with either 20  $\mu$ g RNase A (Sigma) or 50 units RNase H (USB Biologicals) for

3 h at 4 °C, or 25 units Benzonase (EMD Millipore) for 1 h at 4 °C prior to immunoprecipitation. In antibody competition experiments, anti-*DDX1* or anti-*RIF1* antibodies were pre-incubated with 0.25  $\mu$ g/ml recombinant *DDX1* (amino acids 1–186) for 2 h at 4 °C prior to immunoblotting.

To compare the relative portion of *DDX1* and *RIF1* in soluble lysate versus insoluble nuclear matrix, HeLa cells were lysed in lysis buffer as described above for immunoprecipitation, followed by centrifugation at 15,000 rpm for 15 min at 4 °C. The pellets were boiled in 1X SDS loading buffer. One percent of the lysates and ten percent of the insoluble nuclear matrix were resolved on SDS-PAGE gels, transferred to nitrocellulose membranes and immunoblotted with anti-*DDX1* and anti-*RIF1* antibodies.  $\beta$ -tubulin served as the marker for the soluble fraction. Histone 3 served as the marker for the chromatin-bound fraction.

To map the *RIF1* domain required for *DDX1*-*RIF1* interaction, HEK293 cells were transfected with FLAG-tagged *RIF1* constructs using polyethylenimine (PEI) (Polysciences Inc.) in a ratio of 5  $\mu$ g PEI to 1  $\mu$ g DNA. Whole cell lysates were prepared 48 h after transfection and incubated with anti-*DDX1* antibody. Immunoprecipitates were resolved in a 10% acrylamide SDS gel and immunostained with mouse anti-FLAG antibody (1:3000, Sigma).

### 2.3. Plasmids and constructs

The plasmid pLPC-*RIF1* containing full-length *RIF1* cDNA was a gift from Dr. Titia de Lange (Rockefeller University) through Dr. Sara Buonomo (Mouse Biology Unit, EMBL). To map the *RIF1* domain required for *DDX1*-*RIF1* interaction, fragments of *RIF1* cDNA were PCR-amplified with Fidelity polymerase (USB Biologicals) using pLPC-*RIF1* as template. The PCR products were subcloned into p3XFLAG-Myc-CMV (Sigma-Aldrich) and sequenced to ensure that there were no mutations in the constructs.

### 2.4. siRNA knockdown

Knockdown of *DDX1* and *RIF1* was carried out using two different siRNAs for each target: *DDX1* si1 (CAGGCUGAAUCUAUCCCAUUGAUCU), *DDX1* si2 (UACACCAUGUUGUUGUCCAGUAAA), *RIF1* si1 (AGACGGUGCUCUAUUGUUA) and *RIF1* si2 (GGAGCAGCUUAUGACUACUAAAUA). 53BP1 knockdown was carried out using TP53BP1 si (GAGACAGAUGAUCCUUA). Scrambled siRNAs (Medium GC and Low GC negative controls) served as negative controls. All siRNAs including scrambled controls were purchased from Thermo Fisher Scientific. Transfection of siRNAs was carried out with Lipofectamine™ RNAiMAX (Thermo Fisher Scientific) at a final siRNA concentration of 10 nM. Cells were analyzed 72 h after siRNA transfection. To examine the effects of *DDX1* and *RIF1* knockdown on the cell cycle profile, cells were fixed in 70% ethanol and stained with propidium iodide 72 h after siRNA transfection. Flow cytometry analysis was performed using FACScalibur (BD Biosciences).

### 2.5. Fluorescence microscopy

Cells adhering to coverslips were fixed and processed as previously described [18]. For immunostaining with anti-RPA and anti-BLM antibodies, cells were pre-extracted in CSK buffer (10 mM PIPES pH 6.8, 300 mM sucrose, 100 mM NaCl, 3 mM MgCl<sub>2</sub>, and 0.5% Triton X-100) for 5 mins at 4 °C prior to fixation. The following antibodies were used for immunostaining: mouse anti-53BP1 (1:2000, BD Biosciences), rabbit anti-*BLM* (1:200, Bethyl Laboratories), rabbit anti-CENPF (1:4000, a gift from Dr. Gordon Chan), rabbit anti-*DDX1* (batch 2923; 1:1000) [34], mouse anti-FLAG (1:2000, Sigma), mouse anti- $\gamma$ -H2AX (1:4000; EMD Millipore), mouse anti-RPA (1:500, Abcam), and mouse anti-SMN (1:2000, BD Biosciences). Four different anti-*RIF1* antibodies were used to characterize IR-induced *RIF1*-foci: rabbit anti-*RIF1*

(1:2000, a gift from Dr. Weidong Wang, NIH); rabbit anti-RIF1 (1:500, Bethyl Laboratories); mouse anti-RIF1 (1:200, SC-515573, Santa Cruz Biotechnologies) and goat anti-RIF1 (1:200, SC-99579, Santa Cruz Biotechnologies). Cells were synchronized by double thymidine block as described previously [35]. Cells in G1, S and G2 phases were examined 11 h, 3 h and 8 h after release from the 2nd thymidine block. As a second approach, cells in S/G2 phases were identified using Cyclin A or centromere protein-F (CENPF) as a marker. All immunostaining experiments were carried out by incubating cells with primary antibodies for 1 h at room temperature, followed by Alexa 488-, Alexa 555- or Alexa 647-conjugated secondary antibodies (Thermo Fisher) for 1 h at room temperature. Coverslips were mounted onto slides in polyvinyl alcohol (Calbiochem)-based mounting medium containing 1 µg/ml 4',6'-diamidino-2-phenylindole (DAPI). For antibody competition experiments, the anti-DDX1/RIF1 antibody mixture was incubated with 0.25 µg/ml recombinant DDX1 (amino acids 1–186) for 2 h at 4 °C before immunostaining.

RNase A or RNase H treatment was performed as described [18]. Briefly, irradiated cells were permeabilized in 2% Tween for 10 mins at room temperature, followed by treatment with RNase A (1 mg/ml) or RNase H (50 units/ml) for 15 mins at room temperature. Cells were then fixed and immunostained.

To quantify IR-induced DDX1 and RIF1 foci, immunofluorescence images were first captured in a blinded fashion on a Zeiss LSM710 confocal laser scanning microscope with a plan-Apochromat 40X (NA 1.3) oil immersion lens using ZEN software. Image stacks (z-series) were used to generate images covering the entire nuclei. Images were then deconvolved using Huygens Essential software (Scientific Volume Imaging, Hilversum, Netherland) and three-dimensionally reconstituted with Imaris software (Version 7.7.2, Bitplane AG, Zurich, Switzerland). Co-localization analysis of DDX1 and RIF1 foci was performed using the “spot co-localization” function of Imaris. For each experiment, a minimum of 30 cells were 3D-reconstituted and analysed for each phase of the cell cycle, with a total of three experiments conducted. To quantify IR-induced RPA and BLM foci, immunofluorescence images were taken from a single focal plane and exported as TIFF files using ZEN software. Foci quantification was carried out using Imaris software as previously described [19]. A minimum of 100 cells were analyzed for each condition tested in each experiment, with experiments carried out three times unless otherwise specified.

## 2.6. Measurement of HR and NHEJ efficiency

HR and NHEJ efficiency was measured using the U2OS DR-GFP [36] and U2OS EJ5-GFP [37] cell lines, respectively. Cells were first transfected with gene-specific siRNAs (*DDX1*, *RIF1*, or both) or scrambled siRNAs using the Lipofectamine RNAiMAX reagent. Seventy-two h after siRNA transfection, cells were split and incubated at 37 °C for 24 h. Cells were then trypsinized and resuspended in GenePulser Electroporation Buffer (Bio-Rad). Five million cells were electroporated with 10 µg of pCBA Sce or control plasmids together with 100 pmole siRNA using a GenePulser II electroporator (Bio-Rad) set at 280 V and 975 µF. Cells were harvested 48 h after electroporation and GFP-positive cells were quantified using an Influx<sup>®</sup> cell sorter (BD Biosciences). To examine transfection efficiency of control and knock-down cells, cells were split 48 h post-siRNA transfection and transfected with 10 µg pEGFP-C1 plasmid. GFP-positive cells were quantified 48 h post plasmid transfection.

## 2.7. Clonogenic survival assay

For colony formation upon IR treatment, U2OS cells were transfected with *DDX1*, *RIF1* or control siRNAs as described above. Cells were plated and  $\gamma$ -irradiated on the same day. Ten days after IR, the plates were washed with PBS and colonies stained with 1% crystal violet in 70% ethanol for 30 mins at room temperature. Colonies were

counted with a Colcount<sup>®</sup> colony counter (Oxford Optronix) using 30 cells as the threshold. For aphidicolin and camptothecin treatment, U2OS cells transfected with *DDX1*, *RIF1* or control siRNAs were plated. Twenty four h after plating, cells were incubated with the indicated concentrations of aphidicolin for 24 h or camptothecin for 1 h. Drugs were then removed, followed by a PBS wash and addition of fresh medium. Colonies were counted nine days after drug treatment.

## 2.8. Cell fractionation and western blot analysis

To analyze loading of DDX1, RIF1 and BLM to chromatin after DSB formation, soluble and chromatin-bound cellular fractions were prepared as described [10]. Briefly, cells were exposed to 5 Gy IR and lysed 1 h later in NETN buffer [20 mM Tris-HCl pH 8, 100 mM NaCl, 1 mM EDTA, 0.5 mM DTT, 0.5% NP-40, 1X Complete protease inhibitor (Roche)] at 4 °C. After centrifugation, the supernatant served as the soluble fraction and the pellet (chromatin-bound fraction) was lysed in 1X SDS loading buffer. Thirty µg of soluble or chromatin-bound fractions were resolved by SDS-PAGE, transferred to nitrocellulose membranes and immunoblotted with anti-BLM, anti-DDX1 and anti-RIF1 antibodies.  $\beta$ -tubulin served as the marker for the soluble fraction. Histone 3 served as the marker for the chromatin-bound fraction. Densitometric scanning was carried out on western blot film, with Photoshop software used for quantification of band intensities. Same size areas were quantitated for each band, with background pixels subtracted.

## 3. Results

### 3.1. Identification of RIF1 as a DDX1-interacting protein

To identify proteins that interact with endogenous DDX1, we immunoprecipitated DDX1 from HeLa whole cell extracts using a previously validated anti-DDX1 antibody (Ab-1, batch 2910) [18,34]. Immunoprecipitated proteins were separated by SDS-PAGE followed by colloidal Coomassie Blue staining. A high molecular weight band (> 250 kDa) was consistently detected in multiple co-immunoprecipitations (Fig. 1a). This band was cut out from the gel and subjected to in-gel digestion with trypsin. The digested peptides were separated by HPLC, followed by LC/MS/MS analysis for protein identification. RIF1, the human ortholog of yeast Rif1 protein involved in regulation of telomere length, was identified in three independent co-immunoprecipitation experiments. Human RIF1 has been shown to be recruited to DSB sites through 53BP1, where it suppresses end resection and promotes 53BP1-dependent NHEJ [7–11,38]. In addition, RIF1 plays a critical role in the regulation of the timing of genome replication in both mammalian and yeast cells [39–41]. RIF1 was also identified as a DDX1 binding protein using a different anti-DDX1 antibody (Ab-2, batch 2923) [18,19,34] (Supplemental Fig. S1)

We confirmed that RIF1 is found in the same complex with endogenous DDX1 using anti-DDX1 antibody for co-immunoprecipitation, followed by western blot analysis with an anti-RIF1 antibody (Fig. 1b). DDX1 was also identified in reciprocal co-immunoprecipitations using an anti-RIF1 antibody (Fig. 1c). These results indicate a strong interaction between DDX1 and RIF1 and/or that a significant proportion of DDX1 is associated with RIF1. To exclude the possibility that co-immunoprecipitation of DDX1 with RIF1 was due to antibody cross-reactivity, we pre-incubated anti-DDX1 or anti-RIF1 antibodies with a recombinant DDX1 peptide (amino acids 1–186, the immunogen used to generate the DDX1 antibody) prior to immunoblotting. This competitor peptide completely eliminated the DDX1 signal but had no effect on RIF1 (Fig. 1d), confirming the specificity of our DDX1 antibody.

Previously, Cornacchia et al. [41] reported that a significant portion of RIF1 remains associated with the insoluble nuclear matrix after protein extraction. We therefore examined RIF1 and DDX1 levels

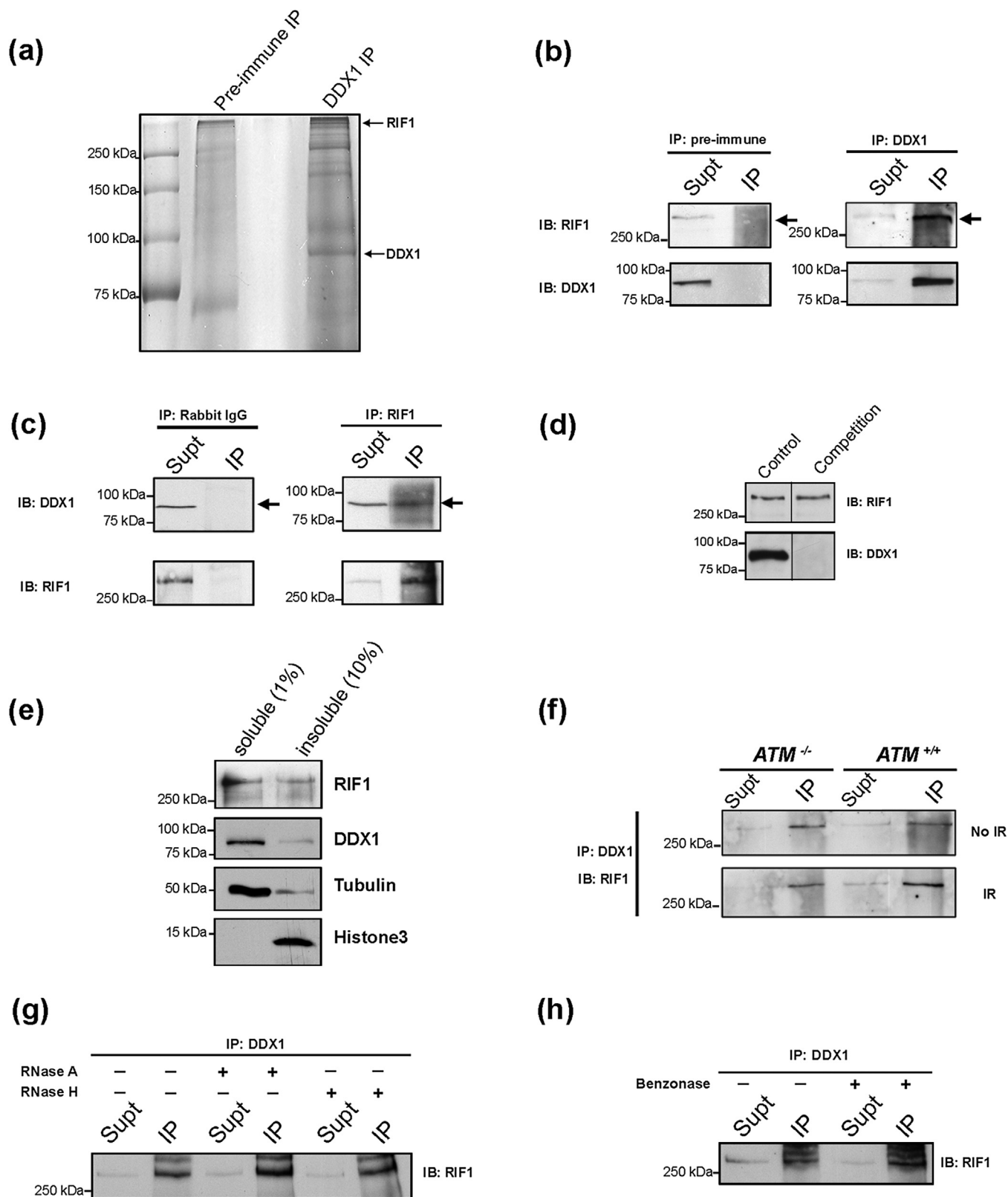


**Fig. 1.** DDX1 co-immunoprecipitates with RIF1. (a) Colloidal Coomassie Blue G-250 staining of a large-scale co-immunoprecipitation carried out using HeLa whole cell lysates and either anti-DDX1 antibody (batch 2910) or pre-immune serum. Bands indicated by arrows were subjected to in-gel digestion followed by LC/MS/MS for protein identification. (b, c) Reciprocal co-immunoprecipitations were carried out using HeLa whole cell lysates and anti-DDX1 (b) or anti-RIF1 (c) antibodies, followed by immunoblotting with anti-RIF1 and anti-DDX1 antibodies. Arrows point to the RIF1 band (b) and the DDX1 band (c). (d) HeLa whole cell lysates were immunoblotted with anti-DDX1 or anti-RIF1 antibodies that had been pre-incubated with 0.25  $\mu$ g/ml recombinant DDX1 peptide (right lane), or without competitor peptide (left lane). (e) Western blot of HeLa whole cell lysates (soluble) and insoluble nuclear matrix using the indicated antibodies. (f) Whole cell lysates prepared from ATM-positive BT and ATM-negative L3 lymphoblastoid cells with or without 5 Gy IR treatment were co-immunoprecipitated using anti-DDX1 antibody and immunostained with anti-RIF1 antibody. (g) HeLa whole cell lysates were incubated with 20  $\mu$ g of RNase A, or 50 units of RNase H, or mock treated for 3 h at 4  $^{\circ}$ C. Immunoprecipitation was carried out using anti-DDX1 antibody as described above. (h) HeLa whole cell lysates were incubated with 25 units of Benzonase for 1 h at 4  $^{\circ}$ C, followed by immunoprecipitation with anti-DDX1 antibody.

present in the soluble and insoluble fractions after whole cell lysis. The soluble fraction was prepared under the same conditions used for the preparation of whole cell lysates for immunoprecipitation. The pellet obtained after centrifugation (insoluble fraction) was solubilized by boiling in 1X SDS loading buffer. As shown in Fig. 1e, the majority of RIF1 and DDX1 was found in the soluble fraction. This inconsistency with Cornacchia et al. [41] is likely due to the fact that these investigators used considerably less detergent (0.5% Triton-X-100) in the preparation of their soluble fraction.

Both DDX1 and RIF1 have previously been shown to be dependent on ATM kinase activity to accumulate at DNA DSBs [18,38]. We therefore asked whether ATM is also required for DDX1-RIF1 interaction. Co-immunoprecipitations were carried out with lysates prepared from BT (ATM-proficient) and L3 (ATM-deficient) lymphoblastoid cell lines. DDX1-RIF1 co-immunoprecipitation was observed in both cell lines, indicating that ATM is not required for DDX1-RIF1 interaction. Furthermore, DDX1-RIF1 were co-immunoprecipitated in both the presence and absence of IR (Fig. 1f) suggesting that at least a portion of DDX1 and RIF1 may constitutively reside in the same cellular complex.

Previous findings indicate that the interaction between DDX1 and some proteins are mediated through nucleic acids [26,42]. We therefore treated HeLa cell lysates with either RNase A (degrades single strand RNAs), or RNase H (removes RNA from RNA-DNA duplexes), or benzonase nuclease (degrades all forms of DNA and RNA), followed by co-immunoprecipitation with anti-DDX1 antibody. As shown in Fig. 1g and h, approximately the same amount of RIF1 was co-immunoprecipitated under all conditions tested, suggesting that DDX1-RIF1 interaction is not mediated through nucleic acids.

### 3.2. Characterization of DDX1 and RIF1 co-localization during cell cycle

DDX1 forms discrete nuclear bodies that frequently co-localize with, or reside adjacent to other nuclear bodies such as Cajal bodies [34,35]. To examine the spatial relationship between DDX1 and RIF1, we co-immunostained HeLa cells using anti-DDX1 and anti-RIF1 antibodies. DDX1 co-localized with RIF1 in the nuclear bodies of unirradiated cells (Fig. 2a). In cells treated with IR, ~90% of IR-induced DDX1 foci co-localized with RIF1 foci (Fig. 2b). Competition experiments using recombinant DDX1 peptide (amino acids 1–186) obliterated the DDX1 signal in both IR-induced foci and nuclear bodies (Fig. 2b and data not shown). In contrast, the DDX1 peptide had no effect on RIF1 immunostaining, again demonstrating the lack of cross-reactivity between anti-DDX1 and anti-RIF antibodies.

As both DDX1 and RIF1 foci were found in the majority of cells, this suggests that DDX1-RIF1 co-localization at DSBs is not restricted to specific phases of the cell cycle. IR-induced DDX1 foci are found throughout the cell cycle [18]; however there are conflicting reports regarding RIF1 localization to DSBs during the cell cycle. For example, one report indicates that IR-induced RIF1 foci are primarily found in G1 phase, with RIF1 foci observed in ~20% of S/G2 cells [9]. However, another report indicates that RIF1 is recruited to DSBs in both G1 and S/G2 phases of the cell cycle [6]. To more closely address IR-induced RIF1 foci at different stages of the cell cycle, we irradiated HeLa cells with 5 Gy and co-immunostained the cells with anti-RIF1 antibodies and markers for S/G2 phase [Cyclin A and Centromere protein-F (CENPF)]. Four different anti-RIF1 antibodies were used for this experiment (see Materials and Methods). Our results indicate that RIF1 forms large foci in G1 cells, as previously reported (Fig. 3a). In S/G2 phase, all four RIF1 antibodies revealed two categories of cells, with ~20–30% of cells containing large RIF1 foci similar to those seen in G1, and ~60–70% of cells showing smaller but distinct RIF1 foci (Fig. 3a and data not shown). Overall, ~90% of S/G2 HeLa cells contained at least 10 IR-induced RIF1 foci 1 h post 5 Gy IR. As a second approach, we synchronized HeLa cells by double thymidine block and examined IR-induced RIF1 foci in G1, S and G2 phases. Similar results

were obtained using this method; i.e., RIF1 formed large foci in G1 phase and small foci in the majority of S and G2 phases (Fig. 3b). Taken together, our data indicate that IR-induced RIF1 foci are present in both G1 and S/G2 cells, with an average of  $57 \pm 8$  large foci in G1 cells, and an average of  $43 \pm 12$  foci (mostly small foci) in S/G2 cells.

We next investigated the relationship between DDX1 and RIF1 foci in the context of the cell cycle using synchronized HeLa cells. Co-localization of DDX1 and RIF1 foci was observed from G1 to G2 phases of the cell cycle (Fig. 4a). While the percentage of DDX1 foci co-localizing with RIF1 foci was constant (~90%) throughout the cell cycle (Fig. 4b), we did observe some changes in the percentage of RIF1 foci co-localizing with DDX1, with 80% co-localization observed in G1, and 60% of RIF1 foci co-localizing with DDX1 in S and G2 (Fig. 4c). Co-immunoprecipitation experiments at different stages of the cell cycle revealed similar amounts of RIF1 co-immunoprecipitated with DDX1 (Fig. 4d).

### 3.3. RIF1 is required for DDX1 localization at nuclear bodies and DNA DSBs

We then examined possible interdependence of DDX1 and RIF1 for their subcellular localization. Cells were transfected with different RIF1- or DDX1-specific siRNAs to deplete RIF1 or DDX1, followed by co-immunostaining with anti-RIF1, anti-DDX1 and anti-SMN (marker of Cajal bodies) antibodies. There was general co-localization of all three proteins in Cajal bodies in scrambled (control) siRNA-transfected cells (Fig. 5a and Supplemental Fig. S2a, upper panels). RIF1 depletion by two different siRNAs abolished DDX1 localization to Cajal bodies (Fig. 5a and Supplemental Fig. 2a, lower panels), whereas DDX1 knockdown had little effect on RIF1 localization in nuclear bodies (Fig. 6a). Figs. 5d and 6c demonstrate efficient depletion of RIF1 and DDX1 in siRNA-transfected cells, respectively, with no effect on DDX1 (RIF1-depleted cells – Fig. 5d) or RIF1 (DDX1-depleted – Fig. 6c) levels. These results suggest that RIF1 is required for DDX1 localization to nuclear bodies.

Next, we treated DDX1- and RIF1-depleted cells with 5 Gy IR and co-immunostained the cells with anti-DDX1, anti-RIF1 and anti- $\gamma$ -H2AX (DSB marker) antibodies. RIF1 knockdown eliminated DDX1 foci at DSBs [Fig. 5b, lower panels; identical results were observed with a second RIF1 siRNA (Supplemental Fig. S2b)]. In contrast, DDX1 knockdown had no effect on RIF1 foci at DSBs (Fig. 6b). RIF1 knockdown also resulted in loss of DDX1 localization to DSBs in cells treated with camptothecin, a topoisomerase I inhibitor (Fig. 5c). Taken together, our results indicate that DDX1 requires RIF1 for its localization to both nuclear bodies and DNA DSBs.

Because it has been reported that RIF1 functions downstream of 53BP1 in the DSB response and depends on 53BP1 for recruitment to DSBs [38], we asked whether DDX1 also requires 53BP1 for accumulation at DSBs. 53BP1 was depleted by using a 53BP1-specific siRNA (Fig. 6e) and cells subjected to 5 Gy IR. Similar to what was observed in RIF1 knockdown cells, few IR-induced DDX1 foci formed in 53BP1-depleted cells (Fig. 6d), consistent with the observation that DDX1 functions downstream of RIF1 in DSB response.

### 3.4. Different nucleic acid requirements for DDX1, RIF1 and 53BP1 accumulation at DSBs

We have previously shown that pre-treatment of  $\gamma$ -irradiated cells with RNase H (but not RNase A) dissociates DDX1 from DSBs, suggesting that DDX1 is anchored to DSBs via RNA-DNA heteroduplex structures [18]. In support of a RNA clearance role for DDX1 at DSBs, DDX1 depletion results in elevated levels of RNA-DNA duplexes at DSBs [19]. Others have reported that RNase A pre-treatment reduces the number of IR-induced 53BP1 and MDC1 foci [43,44]. Since RIF1 is required for DDX1 recruitment to DSBs, we examined whether RIF1 relies on RNA-DNA or single-stranded RNA for accumulation at DSBs.

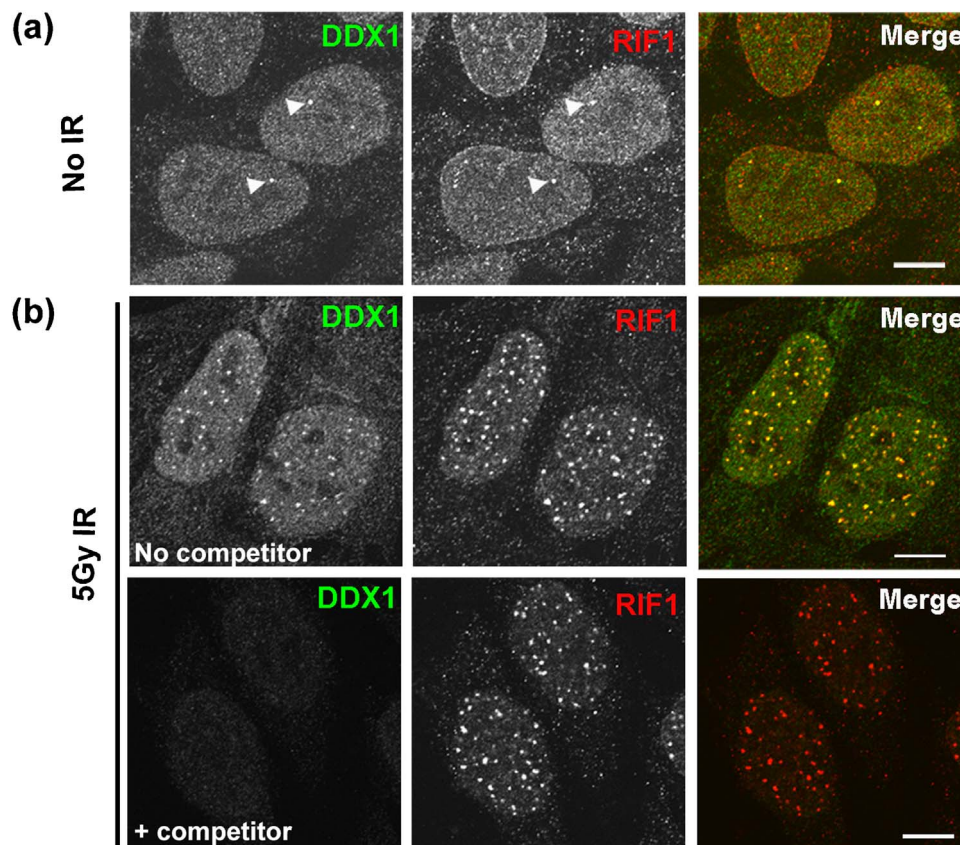


**Fig. 2.** Cellular co-localization of DDX1 and RIF1. (a) HeLa cells were co-immunostained with anti-DDX1 and anti-RIF1 antibodies. Arrowheads point to nuclear bodies where DDX1 and RIF1 co-localize. (b) Upper panels: HeLa cells were treated with 5 Gy IR, allowed to recover at 37 °C for 1 h and co-immunostained with anti-DDX1 and anti-RIF1 antibodies. Lower panels: HeLa cells were treated with IR and co-immunostained with anti-DDX1 and anti-RIF1 antibodies that were pre-incubated with 0.25 µg/ml recombinant DDX1 peptide.

HeLa cells exposed to IR were treated with RNase A or RNase H, followed by co-immunostaining with anti-DDX1 and anti-RIF1 antibodies. Interestingly, RNase A pre-treatment significantly reduced the staining intensity of IR-induced RIF1 foci, but had little effect on DDX1 foci (Fig. 7a). In contrast, RNase H pre-treatment resulted in virtually no change in RIF1 foci, but a significant reduction in DDX1 foci. These results are in agreement with a recent study indicating that RIF1 binds to RNA molecules but not to DNA-RNA duplexes [45]. As previously reported [43,44], pre-treatment with RNase A resulted in a significant reduction in 53BP1 foci intensity, with no effect on DDX1 foci intensity (Fig. 7b). 53BP1 foci have previously been shown not to be affected by RNase H treatment [43]. Taken together, these results indicate that in addition to RIF1 and 53BP1, DDX1 accumulation at DSBs also requires the presence of RNA-DNA hybrids. In contrast, RIF1 and 53BP1 both require single strand RNA for accumulation at damage sites.

### 3.5. RIF1 is critical for DDX1 function in DNA DSB damage response

RIF1 suppresses end resection at DSBs and HR-mediated DSB repair, while promoting 53BP1-dependent NHEJ [7–9,11]. In contrast, our data indicate that DDX1, which resides downstream of RIF1, facilitates HR [19]. To further investigate DDX1's dependence on RIF1 for recruitment to DSBs, and possible interdependence of DDX1 and RIF1 in DSB repair, we compared HR and NHEJ repair efficiencies in DDX1-depleted, RIF1-depleted and DDX1/RIF1-co-depleted cells. Efficiency of HR or NHEJ was measured in the U2OS DR-GFP [36] or U2OS EJ5-GFP reporter cell lines [37], respectively. In these reporter cell lines, a site-specific DSB is introduced within the mutant *GFP* allele by transfection of a construct encoding the I-SceI endonuclease. A functional *GFP* gene is restored if DSB repair occurs via HR (in DR-GFP cells) or NHEJ (in EJ5-GFP cells). Repair efficiency is then quantified by flow cytometry.

Consistent with previous reports [9,10,19], knockdown of DDX1 resulted in a ~2 fold decrease in HR efficiency, whereas RIF1 depletion led to 20–30% increase in HR efficiency (Fig. 8a). In comparison, RIF1/DDX1-co-depleted cells showed ~15% increase in HR efficiency ( $p < 0.05$ ) (Fig. 8a), suggesting that DDX1 relies on RIF1-dependent recruitment to DSBs to carry out its HR-specific role. As HR efficiency is affected by the number of DSBs introduced by the transfected I-SceI endonuclease-encoding construct, we measured the transfection efficiency of control and knockdown cells using a pEGFP construct. There was no significant change in the number of GFP-positive cells in control versus DDX1, RIF1 or double knockdown cells (Supplemental Fig. S3). Thus, the observed changes in HR efficiency upon depletion of DDX1 and RIF1 is not the result of differences in transfection efficiency.

As we previously showed that DDX1 is required for maintenance of the single strand DNA generated by end resection, we further investigated the role of RIF1 in this DDX1-mediated HR process. RPA foci are commonly used to measure single-stranded DNA formed at DSBs after end resection. We therefore counted IR-induced RPA foci in control, DDX1-depleted, RIF1-depleted and DDX1/RIF1-co-depleted cells. As depletion of DDX1, RIF1 or both DDX1 and RIF1 causes some changes in the cell cycle profile [4% decrease, 11% increase and 3% increase in S/G2 phases in DDX1 knockdown, RIF1 knockdown, and DDX1/RIF1 double knockdown cells, respectively (Supplemental Fig. S4)], we co-immunostained cells with anti-CENP-F antibody to specifically examine S/G2 cells (Fig. 8b) when HR predominantly occurs [10,19]. DDX1 depletion reduced the number of IR-induced RPA foci by ~30% in S/G2 cells ( $p < 0.05$ ), consistent with our previous results [19]. In contrast, RIF1 knockdown led to an ~25% increase in RPA foci numbers in S/G2 cells (Fig. 8c). In DDX1/RIF1-co-depleted cells, the number of RPA foci was similar to that in RIF1 knockdown cells ( $p = 0.22$ ) but different from DDX1-depleted cells ( $p < 0.05$ )

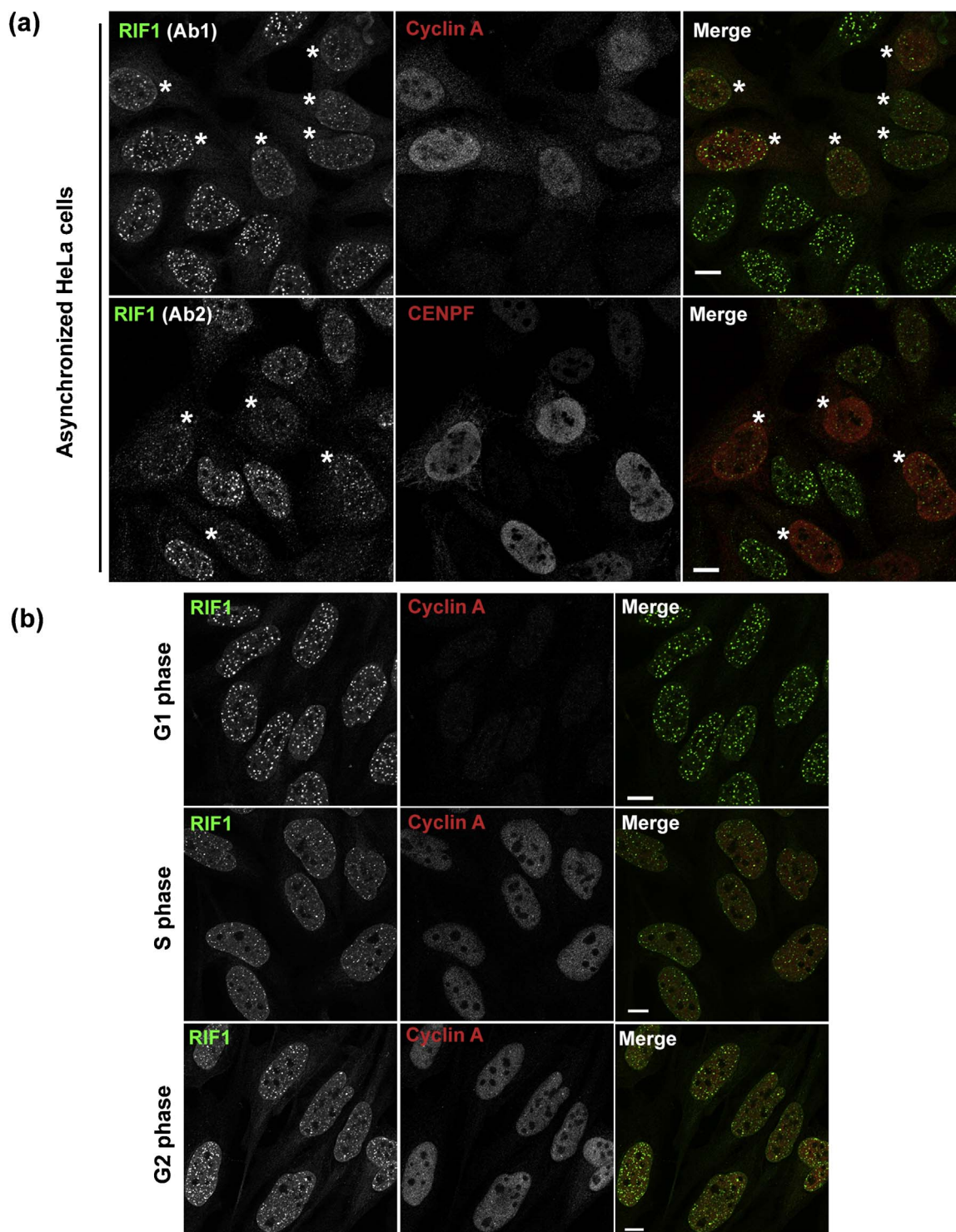


**Fig. 3.** IR-induced RIF1 foci are present throughout the cell cycle. (a) HeLa cells were treated with 5 Gy IR. Cells were fixed 1 h post IR and immunostained with either anti-RIF1 (Ab1, a gift from Dr. Weidong Wang, NIH) and anti-Cyclin A antibodies (top panels), or anti-RIF1 (Ab2: SC-515573, Santa Cruz Biotechnologies) and anti-CENPF antibodies (bottom panels). Cells in S/G2 phases (positive for either Cyclin A or CENPF staining) are marked with asterisks. (b) HeLa cells were synchronized using the double thymidine block. Cells in G1, S or G2 phases were treated with 5 Gy IR, recovered for 1 h and subjected to immunostaining with anti-RIF1 (Ab1) and anti-Cyclin A antibodies. Scale bars: 10  $\mu$ m.

(Fig. 8c), further suggesting that RIF1 acts upstream of DDX1 in DSB repair.

We next examined whether 53BP1 knockdown affects RPA foci numbers at DSBs, since 53BP1 is also important for IR-induced DDX1 foci formation (Fig. 6d). Similar to RIF1 knockdown, depletion of 53BP1 alone led to increased RPA foci numbers ( $p < 0.05$ ) (Fig. 8d). However, unlike RIF1/DDX1 knockdown, cells co-depleted of 53BP1 and DDX1 had RPA foci numbers that were similar to that of DDX1-

depleted cells ( $p = 0.30$ ) but different from that of 53BP1 knockdown cells ( $p < 0.05$ ) (Fig. 8d). As expected, DDX1 knockdown had little effect on NHEJ efficiency ( $p = 0.57$ ) (Fig. 8e), with no significant difference noted between DDX1 single knockdown and RIF1/DDX1 double knockdown cells ( $p = 0.09$ ) (Fig. 8e). Taken together, these data suggest that although both RIF1 and 53BP1 are important for accumulation of DDX1 at DSBs, RIF1, but not 53BP1, is required for DDX1 function in HR as determined by RPA foci numbers.

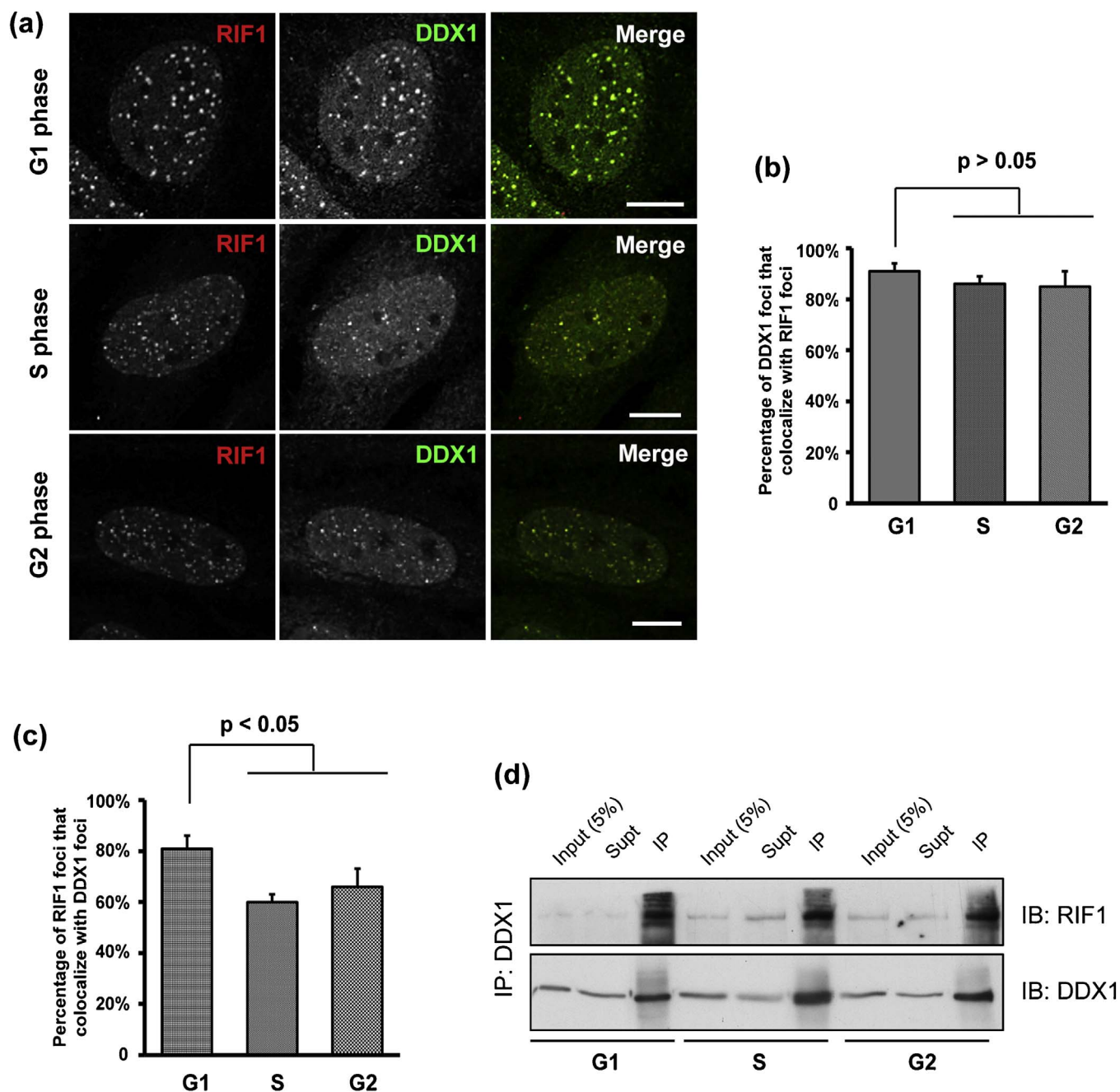


**Fig. 4.** Association between DDX1 and RIF1 during the cell cycle. (a) HeLa cells were synchronized by double thymidine block. Cells in G1, S and G2 phases were treated with 5 Gy IR and immunostained with anti-RIF1 and anti-DDX1 antibodies. Immunofluorescence images were captured by confocal microscopy using z-stacks followed by deconvolution. Scale bars: 10 μm. (b) Percentage of DDX1 foci that co-localize with RIF1 foci in different phases of the cell cycle. Error bars: standard error of the mean. (c) Percentage of RIF1 foci that co-localize with DDX1 foci in different phases of cell cycle. Error bars: standard error of the mean. (d) HeLa cells in G1, S, and G2 phases were treated with 5 Gy IR. Whole cell lysates were prepared 1 h post IR and were incubated with anti-DDX1 antibody. Immunoprecipitates were resolved by SDS-PAGE and immunoblotted with anti-RIF1 and anti-DDX1 antibodies.

We also compared cell survival post IR in DDX1-, RIF1- and DDX1/RIF1-co-depleted U2OS cells using the colony formation assay. RIF1- or DDX1-depletion had similar effects on cell survival after exposure to different doses of IR (Fig. 8f). Depletion of both RIF1 and DDX1 sensitized cells to IR to a similar extent as RIF1 or DDX1 knockdown alone. Of note, when cells depleted of either RIF1 or DDX1 were treated with aphidicolin, a drug that induces replication stress, DDX1 knockdown had a less severe effect on cell survival than either RIF1 knockdown or DDX1/RIF1 double knockdown (Fig. 8g). Since aphidicolin-induced replication fork stalling can eventually lead to DNA DSBs [46], the effect seen upon DDX1 knockdown may reflect its role in DNA DSB repair, whereas the effect seen upon RIF1 knockdown may reflect its dual roles in DNA repair and in promoting recovery of aphidicolin-

induced stalled replication forks [12,47]. Similarly, when RIF1 and/or DDX1-depleted cells were treated with camptothecin, a topoisomerase I inhibitor that causes replication and transcription stress, RIF1 depletion resulted in greater sensitization to IR than DDX1 depletion (Fig. 8h).

### 3.6. Mapping of RIF1 domains required for DDX1-RIF1 association

RIF1 has a HEAT-repeat domain at the N-terminus and a C-terminal domain that contains three conserved subdomains labeled CI, CII and CIII (Fig. 9a) [12,13]. Functional analysis indicates that the N-terminal HEAT-repeats are required for the interaction of RIF1 with 53BP1, whereas the C-terminal domain is essential for interaction with the BLM complex as well as DNA binding [9,12].

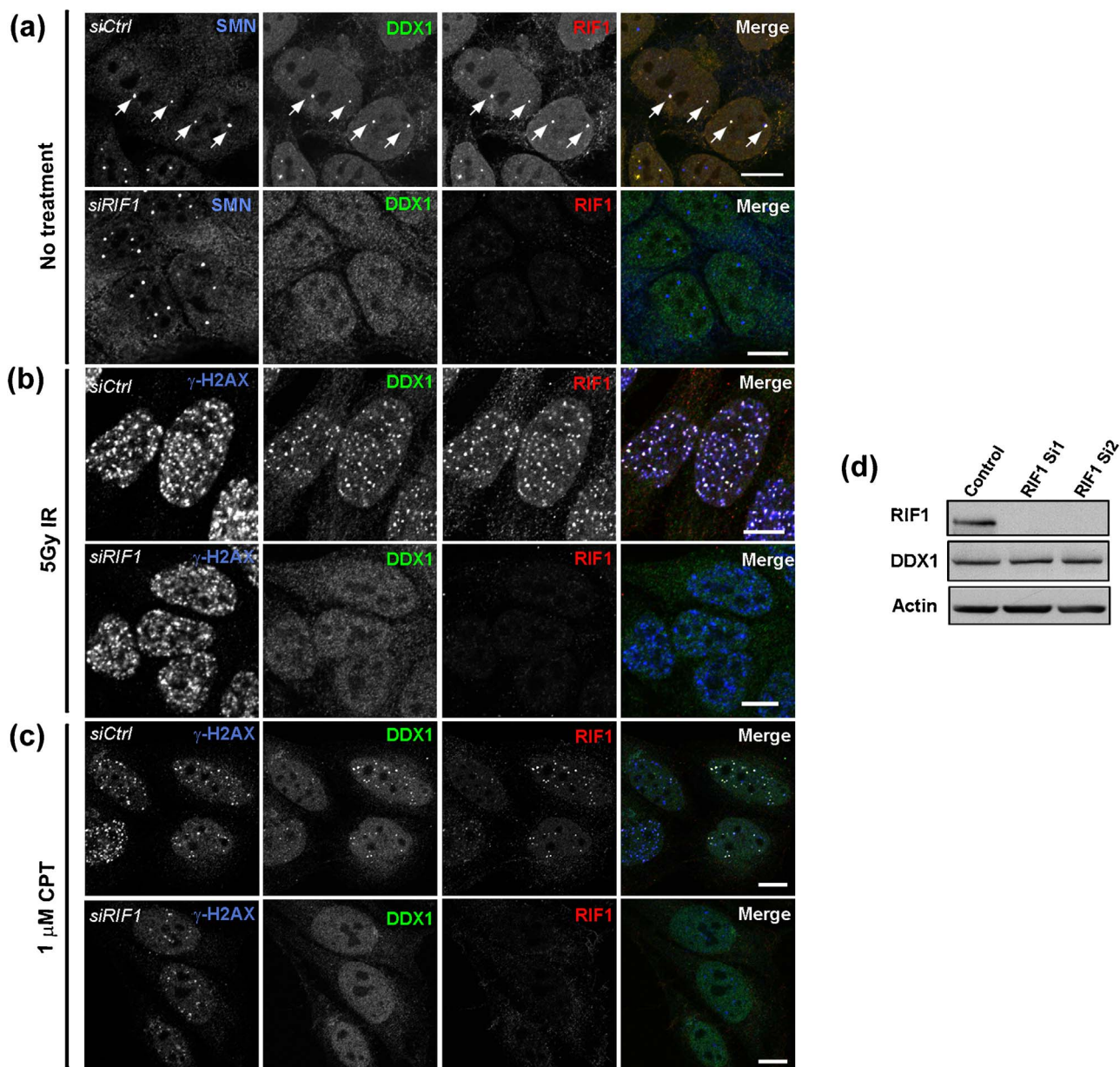


**Fig. 5.** DDX1 requires RIF1 for recruitment to nuclear bodies and DNA DSBs. (a) HeLa cells transfected with RIF1 or scrambled siRNAs were co-immunostained with anti-DDX1, anti-RIF1 and anti-SMN antibodies. Arrows point to nuclear bodies where DDX1, RIF1 and SMN co-localize. (b) HeLa cells transfected with RIF1 or scrambled siRNAs were irradiated with 5 Gy. Cells were fixed 1 h later and co-immunostained with anti- $\gamma$ -H2AX, anti-DDX1 and anti-RIF1 antibodies. (c) HeLa cells transfected with RIF1 or scrambled siRNAs were treated with 1  $\mu$ M camptothecin (CPT). Cells were fixed 2 h later and immunostaining was performed as described in (b). Scale bars, 10  $\mu$ m. (d) HeLa cells were transfected with scrambled siRNAs (control) or siRNAs targeting RIF1. Whole cell lysates were prepared and western blot analysis was performed using the indicated antibodies.

To identify which RIF1 domains are required for its association with DDX1, four FLAG-tagged RIF1 constructs were generated: F1 (aa 1–684), F2 (aa 632–1506), F3 (aa 1506–2002), and F4 (aa 1959–2472) (Fig. 9a). These four FLAG-tagged RIF1 constructs were transfected into HEK293 cells and whole cell lysates were prepared for co-immunoprecipitations using anti-DDX1 antibody followed by western blotting with an anti-FLAG antibody. No association with DDX1 was observed with RIF1 fragments F1 and F2 (Fig. 9b, lanes 1 and 2). However, both RIF1 fragments F3 and F4 co-immunoprecipitated with DDX1 (Fig. 9b, lanes 3 and 4). We then generated two additional constructs, F(3 + 4) and F(3 +  $\Delta$ 4), the latter containing a deletion of part of the CII and all of the CIII subdomains. The combination of fragments F3 and F4 dramatically increased RIF1 binding to DDX1 (Fig. 9b, lane 5). Deletion of the CII and CIII subdomains from the F(3 + 4) construct reduced binding to DDX1 to levels similar to that observed with the F3 or F4 fragments alone (Fig. 9b, compare lanes 6 to

lanes 3 and 4 relative to input).

We also examined the cellular localization of the different RIF1 fragments. When transfected into HeLa cells, all RIF1 fragments showed preferential localization to the nucleus (Fig. 9c). Consistent with the co-immunoprecipitation results, FLAG-tagged RIF F(3 + 4) co-localized with endogenous DDX1 nuclear bodies, whereas the deletion mutant RIF F(3 +  $\Delta$ 4) failed to co-localize with DDX1 (Fig. 9c). In cells treated with either IR or camptothecin, there was co-localization between DDX1 and FLAG-tagged RIF F(3 + 4) (Fig. 9d and e). Co-localization was abolished upon deletion of the CII and CIII subdomains.

### 3.7. DDX1 promotes RIF1-dependent BLM helicase recruitment to DSBs

RIF1 interacts with BLM helicase under replication stress [12]. In irradiated cells, RIF1 recruits BLM to DSBs independently of 53BP1 [10]. At DSBs, BLM stimulates end resection, a key step in HR [48–50].

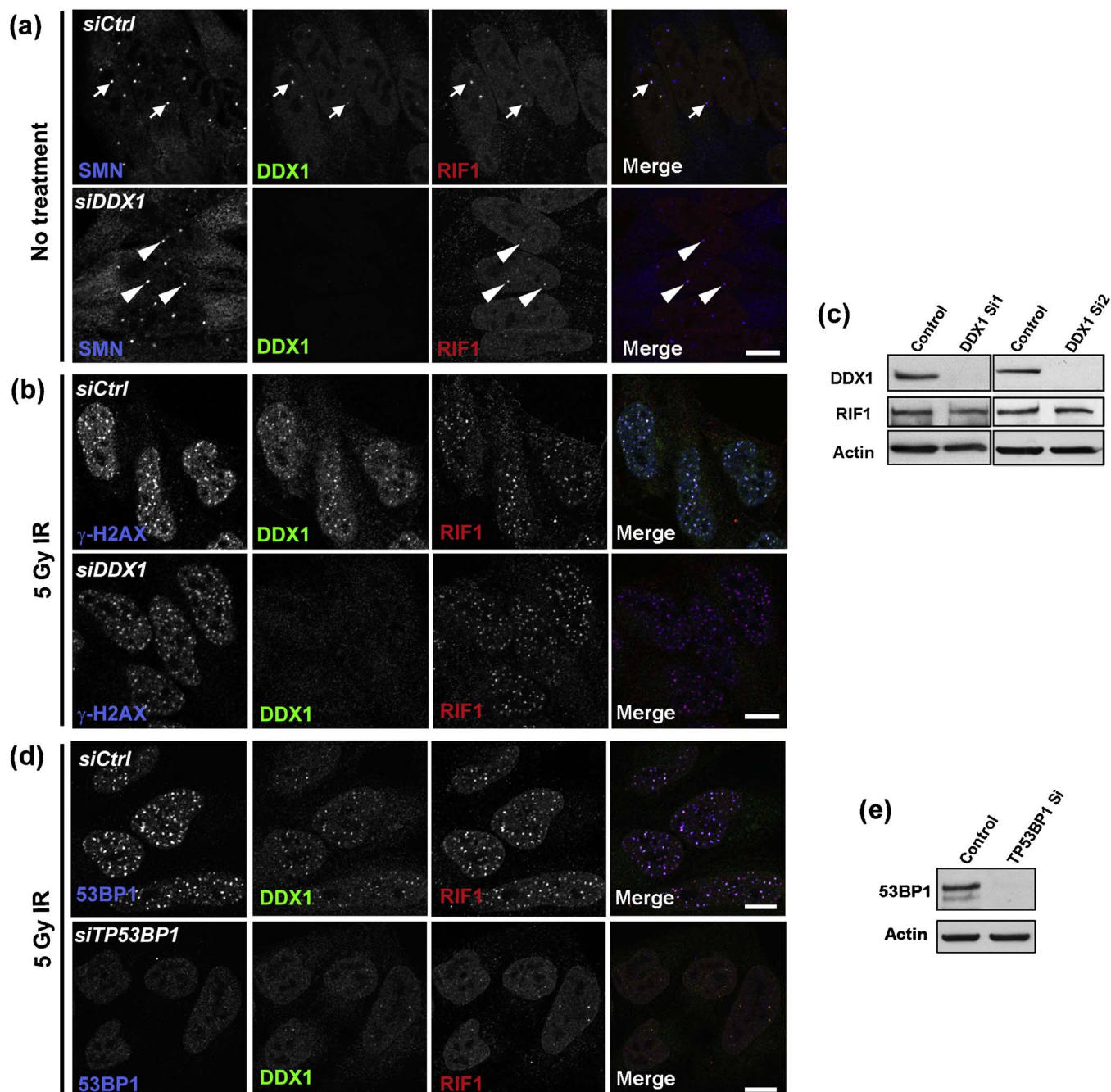


**Fig. 6.** DDX1 is dispensable for RIF1 localization to nuclear bodies and DSBs. (a) HeLa cells transfected with scrambled siRNAs or DDX1 siRNA (DDX1 si1) were immunostained with anti-SMN, anti-DDX1 and anti-RIF1 antibodies. Arrows indicate co-localization of SMN, DDX1 and RIF1 in control cells. Arrowheads point to co-localization of SMN and RIF1 in DDX1 knockdown cells. (b) HeLa cells transfected with scrambled siRNAs or DDX1 si1 were exposed to 5 Gy IR. Cells were allowed to recover for 1 h at 37 °C and immunostained with anti- $\gamma$ -H2AX, anti-DDX1 and anti-RIF1 antibodies. (c) HeLa cells were transfected with scrambled siRNAs (control) or siRNAs targeting DDX1. Whole cell lysates were prepared and western blot analysis was performed using the indicated antibodies. (d) HeLa cells transfected with scrambled siRNAs (control) or siRNA specific to 53BP1 were treated with 5 Gy IR. One h later, cells were co-immunostained with anti-53BP1, anti-DDX1 and anti-RIF1 antibodies. (e) Western blot of HeLa cell lysates prepared from control or 53BP1 knockdown cells. Scale bars: 10  $\mu$ m.

Given that DDX1 also facilitates HR-mediated DSB repair [19], we asked whether DDX1 might also associate with BLM. We carried out co-immunoprecipitations using anti-DDX1 antibody followed by western blot analysis with anti-BLM antibody. While BLM did co-immunoprecipitate with endogenous DDX1, the amount of DDX1-associated BLM protein was lower than that of DDX1-associated RIF1 protein (compare Figs. 1b and 10a). Of note, DDX1-BLM interaction was enhanced approximately 1.5-fold when cells were treated with 5 Gy IR (Fig. 10a). In reciprocal co-immunoprecipitations using anti-BLM antibody, a weak DDX1-BLM association was observed in cells exposed to  $\gamma$ -irradiation (Fig. 10b).

RIF1 regulates BLM recruitment to DSBs and chromatin loading in a 53BP1-independent manner in cells exposed to IR [10]. Since BLM co-immunoprecipitates with DDX1, we asked whether DDX1 can also affect chromatin loading (used as a surrogate marker for DSB localization) of BLM following DNA damage. U2OS cells exposed to 5 Gy IR were fractionated into soluble and chromatin-bound portions, followed by western blot analysis. Consistent with a previous report [10], RIF1 depletion dramatically reduced the levels of BLM bound to chromatin (> 8 fold) (Fig. 10c). In line with the idea that DDX1 recruitment to DSBs is dependent on RIF1, RIF1 knockdown reduced DDX1 binding to chromatin by ~1.6-fold, whereas DDX1 knockdown had no effect on

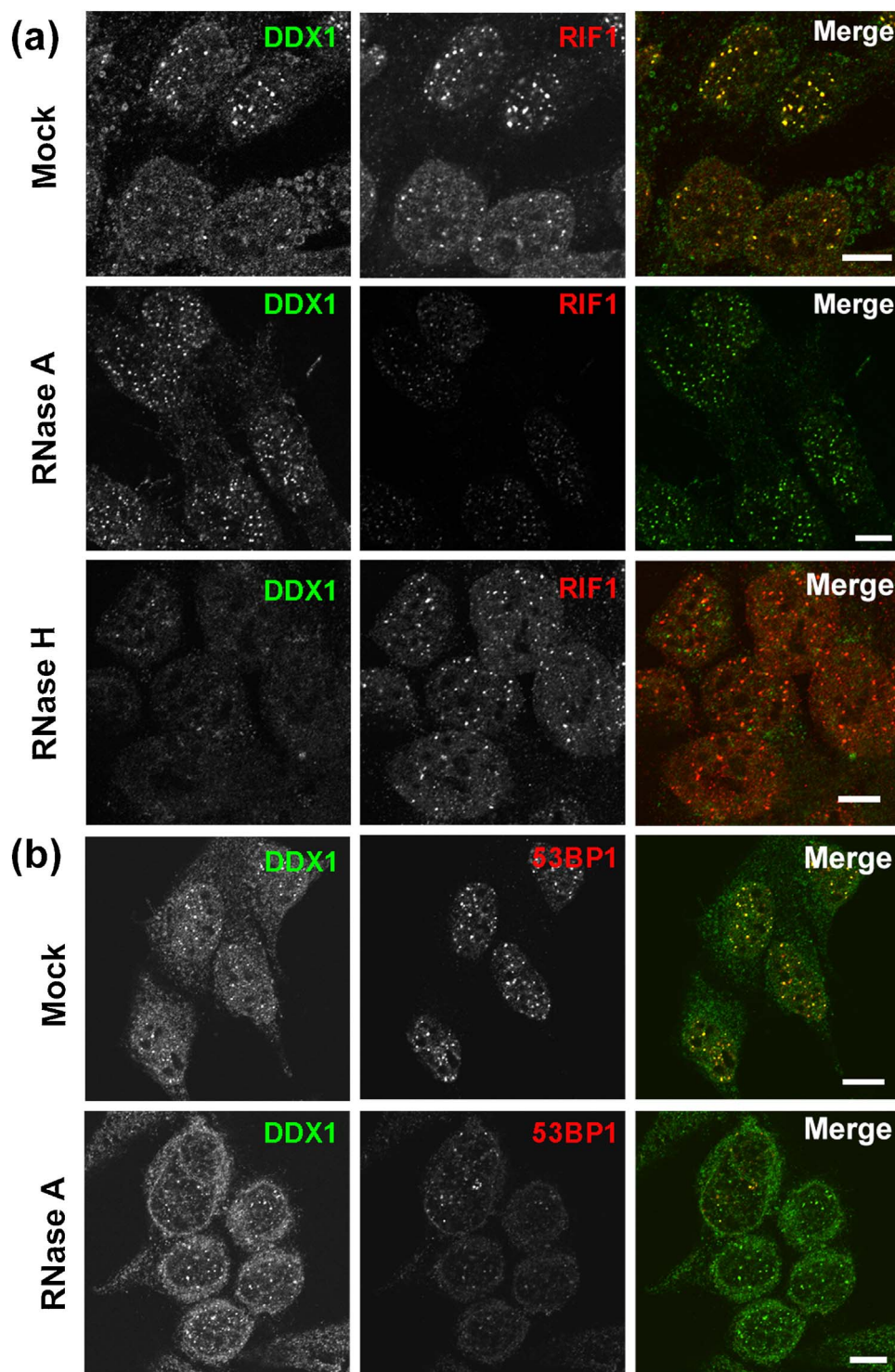


**Fig. 7.** Different structural requirements for accumulation of DDX1, RIF1 and 53BP1 at DSBs. (a) One h after exposure to IR, HeLa cells were permeabilized with 2% Tween-20, followed by incubation with RNase A or RNase H, or mock treated as indicated. Cells were then fixed and co-immunostained with anti-DDX1 and anti-RIF1 antibodies. (b) HeLa cells were treated as described in (a) and co-immunostained with anti-DDX1 and anti-53BP1 antibodies.

amount of chromatin-bound RIF1 post IR (Fig. 10c). Interestingly, DDX1 knockdown also led to a significant reduction ( $\sim 2.5$  fold) in BLM binding to chromatin after IR treatment (Fig. 10c), suggesting that DDX1 affects the recruitment of BLM to DSBs. In DDX1/RIF1 co-depleted cells, chromatin loading of BLM was similar to that of RIF1 knockdown cells (Fig. 10c), suggesting that DDX1 and RIF1 act in the same pathway to recruit BLM. These combined results indicate that DDX1 is involved in RIF1-dependent loading of BLM to chromatin after DSB formation.

We next examined whether DDX1 plays a role in IR-induced BLM foci formation. U2OS cells transfected with control or *DDX1* siRNAs were treated with 10 Gy IR and immunostained with anti-BLM and anti- $\gamma$ H2AX antibodies. Upon IR treatment, BLM formed distinct large and small foci. Large BLM foci were present in 30–40% of cells in both control and DDX1-depleted cells. Only  $\sim 10\%$  of the large BLM foci co-localized with  $\gamma$ -H2AX, with a further 50–60% residing adjacent to  $\gamma$ -H2AX foci. In contrast, general co-localization was observed between the small BLM foci and  $\gamma$ -H2AX foci (Fig. 10d). We therefore focused

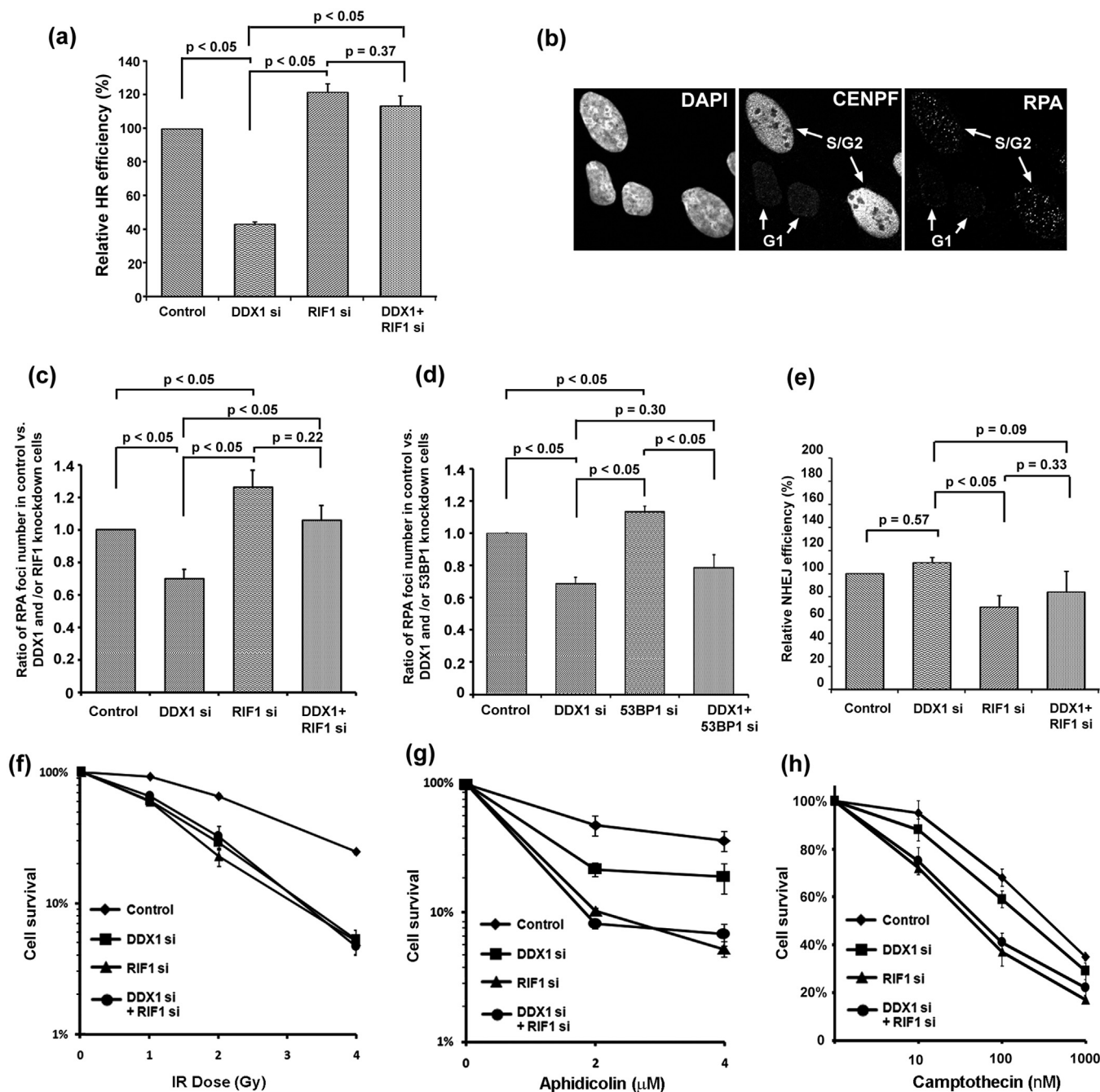


**Fig. 8.** DDX1 requires RIF1-mediated recruitment to DSBs to carry out its function in damage response. (a) U2OS DR-GFP cells were transfected with scrambled siRNAs (control) or siRNAs specific to DDX1, or RIF1, or both DDX1 and RIF1. After 72 h, cells were transfected with the same siRNAs along with the I-Sce I expression construct by electroporation. GFP-positive cells were separated and counted using a BD Influx cell sorter 48 h post-electroporation. Relative HR efficiency was calculated by comparing percentage of GFP-positive cells in gene-specific siRNAs versus control transfectants. (b) U2OS cells were treated with 5 Gy IR. Two h later, cells were extracted, fixed and immunostained with anti-CENPF and anti-RPA antibodies. Cells in S/G2 phases were differentiated from cells in G1 phase by CENPF staining intensity. Note that RPA foci were predominantly found in S/G2 cells. (c) U2OS cells were transfected with scrambled siRNAs or siRNAs specific to DDX1, RIF1, or both DDX1 and RIF1. Cells were irradiated and immunostained as described in (b). RPA foci in S/G2 cells were counted and the ratios of RPA foci in control versus knockdown cells were calculated as indicated. (d) Control, DDX1 knockdown or 53BP1 knockdown U2OS cells were treated as described in (c). Ratios of RPA foci in control versus knockdown cells are indicated. (e) U2OS EJ5-GFP cells were treated as described in (a) and relative NHEJ efficiency was calculated. (f–h) siRNA-transfected U2OS cells were treated with the indicated doses of radiation (f), or concentrations of aphidicolin (g) or camptothecin (h) and cell survival was measured by colony formation assay.  $n = 3$  for all experiments. Error bars: standard error of the mean.

our analysis on the small BLM foci. Compared to control, DDX1 knockdown led to a significant reduction (3–4 fold) in the percentage of cells containing small BLM foci that co-localized with  $\gamma$ -H2AX upon IR treatment (Fig. 10d and e). When combined with the reduced BLM chromatin loading observed in DDX1-depleted cells and the dependence on RIF1 for both DDX1 and BLM recruitment, our data indicate that RIF1-dependent BLM recruitment to DNA damage sites may be mediated by DDX1.

#### 4. Discussion

We have previously shown that DDX1 is recruited to a subset of IR-induced DSBs and facilitates HR by resolving RNA-DNA duplexes found at DSBs in transcriptionally active cells [18,19]. Here, we identify two new DDX1-interacting partners: RIF1 and BLM. Our data indicate a hierarchy among these three proteins in terms of recruitment to DSBs, with RIF1 required for DDX1 recruitment to DSBs, and DDX1 in turn

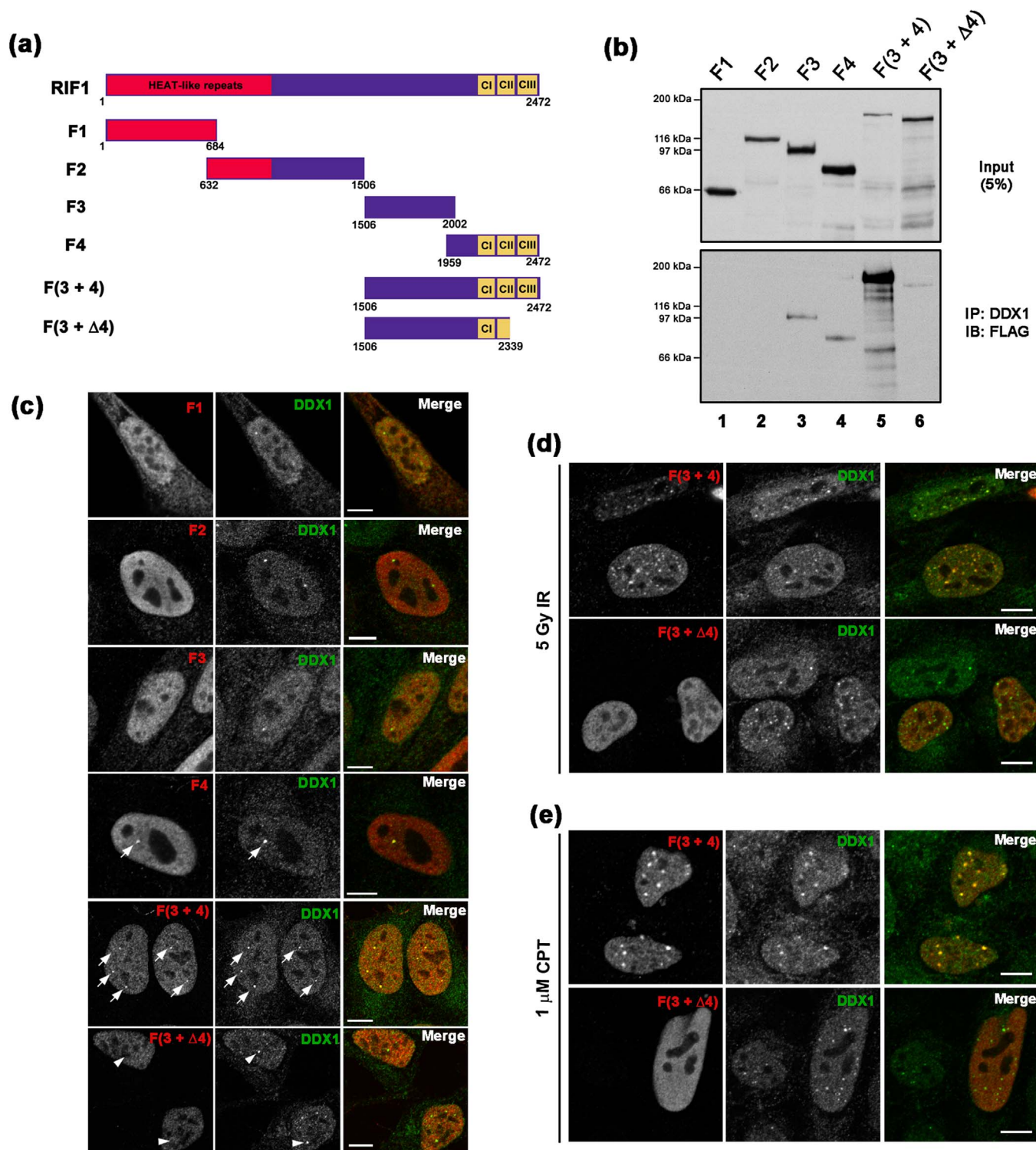


**Fig. 9.** Identification of RIF1 domains that interact with DDX1. (a) Schematic representation of human RIF1 protein and the different truncations used in this study. The three C-terminal subdomains conserved in vertebrates are marked CI-III. (b) The FLAG-tagged RIF1-truncation constructs were transfected into HEK293 cells. Co-immunoprecipitations were carried out with anti-DDX1 antibody, followed by western blotting with anti-FLAG antibody (bottom panel). Input (5% of the whole cell lysates used for the co-immunoprecipitations) is shown in the top panel. Data are representative of two separate experiments. (c) HeLa cells were transfected with Flag-tagged RIF1 constructs. Cells were fixed and co-immunostained with anti-Flag and anti-DDX1 antibodies. Arrows point to nuclear bodies showing co-localization between DDX1 and RIF1 F4 and RIF1 F(3 + 4). Arrowheads indicate DDX1 nuclear bodies that are devoid of RIF1 F(3 + Δ4). (d, e) HeLa cells were transfected with RIF1 F(3 + 4) or RIF1 F(3 + Δ4). Cells were treated with 5 Gy IR (d) or 1 μM camptothecin (e) and subjected to immunostaining with anti-Flag and anti-DDX1 antibodies. Scale bars, 10 μm.

required for maximal RIF1-dependent BLM recruitment to DSBs. As RIF1 has a well-documented role in NHEJ repair, but also interacts with BLM and DDX1, both involved in HR repair, we propose that RIF's interacting partners direct its exact role at DSBs.

#### 4.1. RIF1-dependent recruitment of DDX1 to DSBs

Studies centered on the roles of HR and NHEJ factors at DSBs have resulted in the identification of proteins involved in both pathways

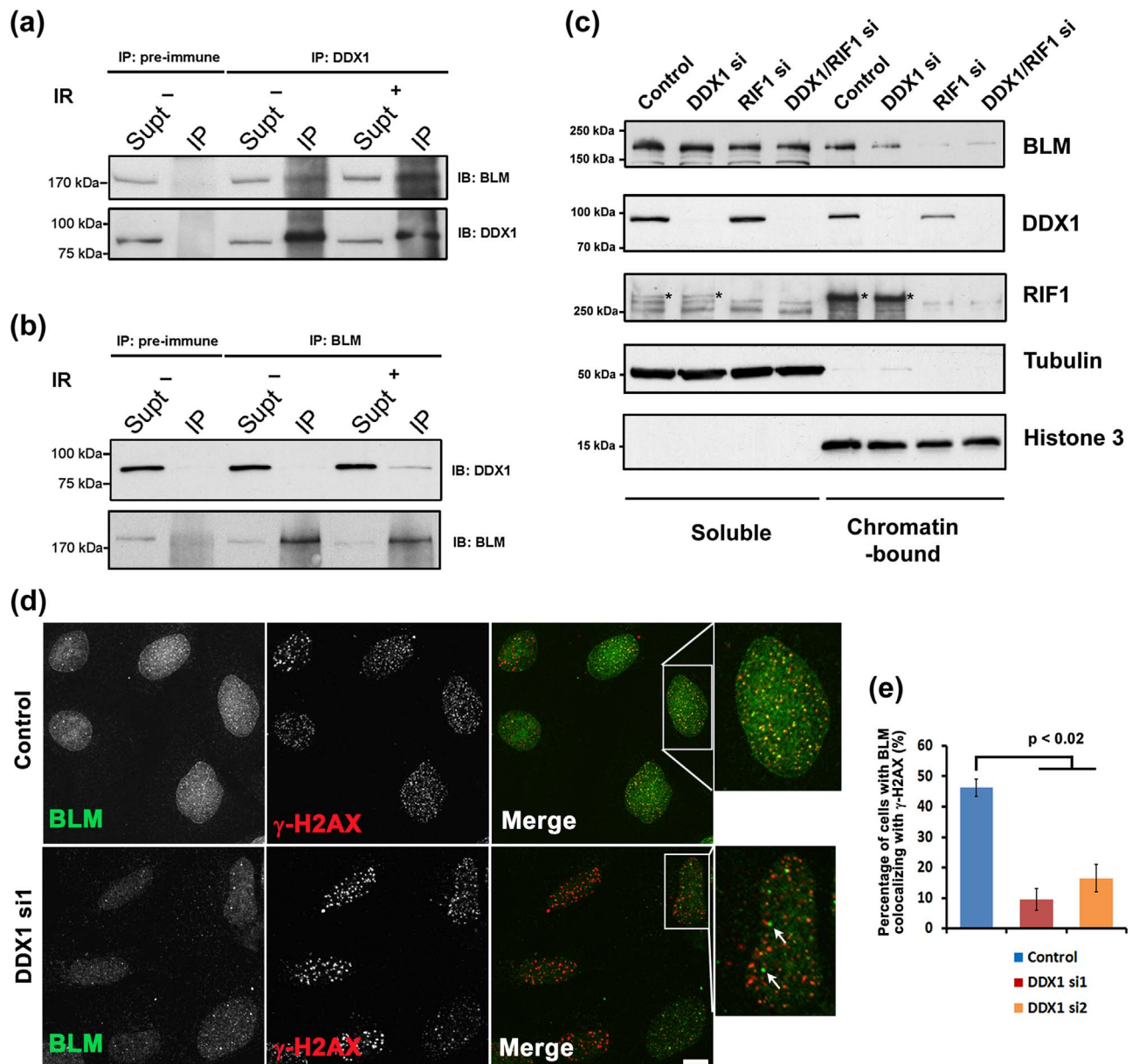


**Fig. 10.** DDX1 mediates RIF1-dependent BLM recruitment to DSBs. (a, b) Reciprocal co-immunoprecipitations were carried out using either anti-DDX1 or anti-BLM antibody and HeLa whole cell lysates. Co-immunoprecipitated proteins were separated by SDS-PAGE, transferred to nitrocellulose and immunostained with anti-BLM and anti-DDX1 antibodies. (c) U2OS cells were transfected with scrambled siRNAs (control) or siRNA specific to DDX1 or RIF1 or both DDX1 and RIF1. Cells were exposed to 5 Gy IR and harvested 1 h later. Soluble and chromatin-bound cellular fractions were resolved by SDS-PAGE, blotted and immunostained with the indicated antibodies. Asterisks indicate RIF1 bands. (d) Control or DDX1-depleted U2OS cells were treated with 10 Gy IR and immunostained with anti- $\gamma$ -H2AX and anti-BLM antibodies 4 h post-IR. Large foci which don't co-localize with  $\gamma$ -H2AX are indicated by arrows. Insets show magnification of individual cells found in the square. Scale bar, 10  $\mu$ m. (e) Histograms showing percentage of cells containing IR-induced BLM foci that co-localize with  $\gamma$ -H2AX foci in control or DDX1 knockdown cells. Percentages are averages of two independent experiments with a minimum of 220 cells analyzed for each condition in each experiment. Error bars: standard error of the mean.

[1,51,52]. For example, ATM can interact with both BRCA1 and 53BP1, thereby affecting their recruitment to DSBs and determining repair pathway choice [53,54]. 53BP1 recruits two downstream effectors, RIF1 and PTIP, to suppress BRCA1-mediated HR and promote NHEJ [6–11]. PTIP is essential for 53BP1-mediated inhibition of end resection in BRCA1-deficient cells. Loss of PTIP mimics 53BP1 deficiency and restores HR in BRCA1 mutant cells [6]. PTIP promotes NHEJ by recruiting the endonuclease Artemis to DSBs [14]. Compared to PTIP, the role of RIF1 in blocking end resection appears more complex. Although essential for class switch recombination in B cells, RIF1 only partially contributes to HR defect in BRCA1-deficient cells, as loss of RIF1 is not sufficient for complete rescue of HR defects caused by BRCA1 inactivation [8–11]. Consistently, RIF1 appears to protect broken ends from initial but not sustained resection [10]. Notably,

RIF1 has been proposed to promote only a subset of DSB repair by NHEJ [6,55]. Moreover, to date, there have been no reports of RIF1 downstream effectors that block end resection and HR. Instead, RIF1 has been shown to recruit BLM to DSBs in a 53BP1-independent manner [10]. Counterintuitively, BLM stimulates rather than blocks end resection [48–50].

At first glance, it seems surprising that RIF1, a factor known for its anti-HR activity, would recruit DDX1, a protein that facilitates HR, to DSBs. However, there is a significant body of work suggesting that RIF1 is a multifunctional scaffold protein able to recruit various factors that function in different DSB repair pathways in a context-dependent manner [7–11,47,55,56]. Given the close association between DDX1 and RIF1 in S and G2 phases when HR takes place, it is possible that DDX1 is recruited by RIF1 to a subset of DSBs to counteract RIF1's

inhibitory activity in HR. This proposed scenario is reminiscent of BRCA1, where BRCA1 interacts with different partners to either promote or inhibit HR [57]. Identification of additional RIF1-interacting proteins and dissection of the functional interplay between these proteins will shed light on the mechanisms by which RIF1 regulates DNA DSB repair.

Although dependent on RIF1 for recruitment, DDX1 appears to have different structural requirements (presence of RNA-DNA hybrids) for retention at DSBs compared to RIF1 (single strand RNA). We and others have shown that RNA/DNA hybrids accumulating at DSBs influence HR efficiency in both human and yeast cells [19,58]. While better known as a player in NHEJ, RIF1 may also play a RNA-dependent role in homology-directed DSB repair [47,59]. In keeping with this possibility, a recent study suggests that classical NHEJ factors, such as 53BP1 and DNA ligase IV, play a role in RNA-templated homology-driven DSB repair at transcribed regions [60]. Given: (i) the importance of transcription for DDX1 recruitment to DSBs, (ii) a requirement for RNA/DNA hybrids for accumulation of DDX1 at DSBs, and (iii) the observed accumulation of RNA at DSBs in DDX1-depleted cells [18,19], combined with: (iv) the importance of RIF1 for DDX1 recruitment to DSBs, (v) the requirement for single-strand RNA for RIF1 accumulation at DSBs, and (vi) the RNA-binding properties of RIF1 and DDX1 [18,19,45], it is plausible that both RIF1 and DDX1 participate in this newly identified form of homology-driven DSB repair.

We show here that DDX1 co-immunoprecipitates with BLM helicase as well as RIF1. Unlike RIF1 which interacts and co-localizes with DDX1 in both DNA damaged and undamaged cells, the interaction between DDX1 and BLM is enhanced after DNA damage, suggesting that increased DDX1-BLM interaction is part of the DNA DSB response. DDX1 depletion decreases BLM loading to chromatin after DNA damage and inhibits BLM foci formation at DSBs, suggesting that DDX1 acts upstream of BLM and regulates BLM activity in response to DSBs. Of note, it has previously been shown that BLM recruitment to DSBs relies on RIF1 but is independent of 53BP1 [10]. The fact that RIF1, but not 53BP1, is required for DDX1 function at DSBs further supports a RIF1-

DDX1-BLM-mediated role in homology-driven DSB repair. We propose a model that attempts to reconcile what is currently known about RIF1, taking into consideration the following known facts: (i) RIF1 inhibits end resection initiation but cannot block end resection extension [10], (ii) DDX1 recruitment to DSBs is downstream of resection initiation and is impaired in cells deficient in resection initiation [19], and (iii) BLM stimulates resection extension but not resection initiation [48,49] (Fig. 11). Based on our model, upon DSB induction, ATM phosphorylates 53BP1, which recruits RIF1 to DSBs. In B cells and other cell lines (e.g., HeLa or U2OS), RIF1 further recruits unidentified downstream factors to suppress end resection initiation at DSBs, thus promoting class switch recombination in B cells and inhibiting classical HR at a subset of DSBs. However, at another subset of DSBs, including breaks that are undergoing active transcription and/or where end resection has already been initiated, RIF1 recruits DDX1 and BLM to damage sites and participates in canonical or non-canonical (e.g., RNA-templated repair) homology-driven DSB repair. It is well-documented in the literature that RIF1's primary role is to suppress end resection at DSBs in G1 phase. Based on our observation that IR-induced RIF1 foci are present in the majority of S/G2 cells, we propose that RIF1 can also inhibit HR at DSBs in S/G2 cells. However, in S/G2, RIF1 can also recruit DDX1 and BLM to a subset of DSBs, allowing extension of end resection and HR repair at these sites. As a result, in RIF1-depleted cells where both RIF1-dependent pathways are impaired, the overall DSBs repair is shifted towards HR, which is manifested by enhanced end resection and HR efficiency.

The N-terminus of RIF1 contains multiple HEAT repeats that are common to all RIF1 orthologues. A C-terminal domain consisting of three subdomains is unique to vertebrates [12,13]. The N-terminal HEAT repeats are required for RIF1-53BP1 interaction whereas the C-terminal domain confers resistance to DNA replication stress and is important for interaction with BLM helicase [9,12]. Here, we show that the C-terminal F(3 + 4) region of RIF1 is required for DDX1-RIF1 interaction. Of note, the last 133 amino acids (aa 2340–2472; CIII and part of CII) of RIF1 appear to be particularly important for maximal

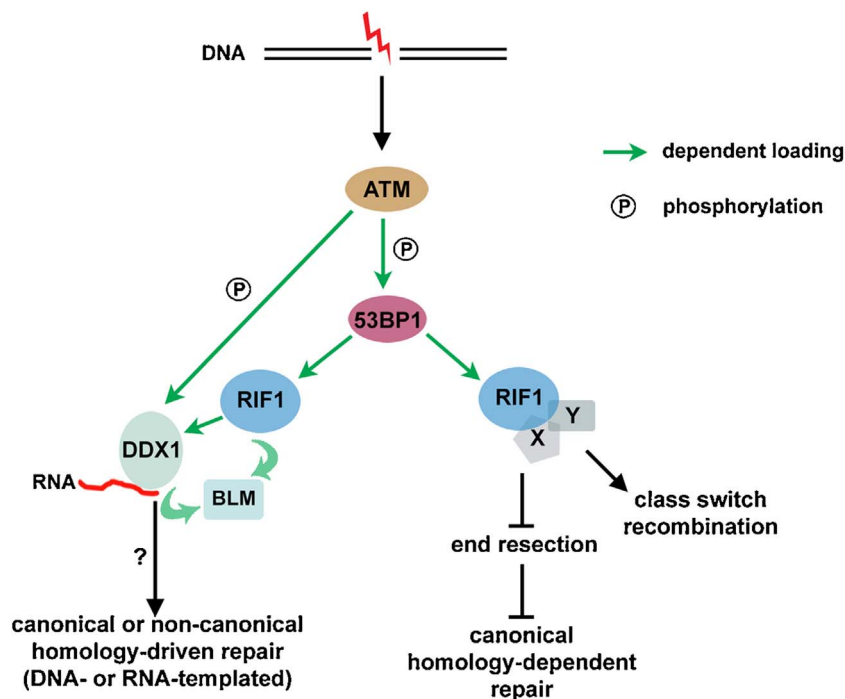


**Fig. 11.** A model depicting the role of RIF1-DDX1-BLM in DSB repair. Upon DSB formation, ATM phosphorylates 53BP1, which results in RIF1 accumulating at DSBs. In turn, RIF1 recruits unidentified downstream targets (X and Y) that block end resection initiation at DSBs, thus inhibiting canonical HR. However, at a subset of DSBs (e.g., DSBs located within actively transcribed region and/or where resection has already been initiated), RIF1 recruits DDX1 and BLM, where it participates in either canonical or non-canonical (e.g., RNA-templated repair) homology-driven repair. Dependence of ATM on DDX1 recruitment to DSBs is based on Li et al. [18] and dependence of RIF1 and 53BP1 on DDX1 recruitment is based on this work. Dependence of ATM and 53BP1 for loading of RIF1 to DSBs is based on Silverman et al. [38].

interaction with DDX1. These 133 amino acids are conserved across vertebrates and contribute to the DNA-binding activity of RIF1 [12]. As mammalian and yeast RIF1 display different cellular localization and *Drosophila* RIF1 does not respond to DNA damage [13,38,61], the vertebrate-unique C-terminal domain of RIF1 is likely critical to its DNA repair function.

#### 4.2. DDX1 mediates BLM chromatin loading and foci formation

BLM has been shown to play multiple roles at DSBs, including stimulation of end resection at DNA DSBs and dissolution of double Holliday junctions [48,50,62,63]. The single strand DNA binding protein, RPA, directly interacts with BLM and increases its helicase activity [64]. RPA-BLM interaction is crucial for both BLM-dependent end resection and double Holliday junction dissolution [49,65]. Since DDX1 depletion impairs RPA accumulation at DSBs [19], it's possible that DDX1 promotes RIF1-dependent BLM loading at DSBs through RPA proteins. As DDX1 resolves RNA-DNA duplexes formed in the vicinity of DSBs [19], a second possibility is that DDX1 facilitates BLM helicase binding to DNA substrates by resolving unfavorable nucleic acid structures. Future biochemical analysis with purified DDX1 and the BLM complex will shed light on how DDX1 regulates BLM activity.

In summary, we have shown that RIF1 is required for both DDX1 accumulation at a subset of DSBs and DDX1 function in homology-driven repair. Recruitment of DDX1 in turn promotes RIF1-dependent but 53BP1-independent loading of BLM at DSBs. Our data suggest that while the primary role of RIF1 in DSB repair is to suppress end resection and promote NHEJ, RIF1 can also recruit factors (such as DDX1 and BLM) that facilitate HR at a subset of DSBs. These results may explain, at least in part, why inactivation of RIF1 does not fully mimic 53BP1 ablation in the restoration of HR defects in BRCA1-deficient cells.

#### Conflicts of interest

None of the authors involved in the preparation of this manuscript have any conflicts of interest to report.

#### Acknowledgements

We thank Elizabeth Blackburn, Titia de Lange, Sara Buonomo, and Lifeng Xu for providing constructs containing full-length *RIF1* cDNA, Maria Jasin and Jeremy Stark for U2OS DR-GFP and U2OS EJ5-GFP cell lines, Susan Lees-Miller for ATM-positive and ATM-negative cell lines, Weidong Wang for anti-RIF1 antibody and Gordon Chan for anti-CENPF antibody. We are indebted to Ismail Ismail and Sachin Katyal for helpful comments. We are grateful to Xuejun Sun and Gerry Barron for advice on confocal image acquisition and data analysis using Imaris and Huygens Essential software. This work was supported by grants from the Alberta Cancer Foundation and the Canadian Breast Cancer Foundation. D.G. was a recipient of an Alberta Innovates – Health Solutions graduate studentship.

#### Appendix A. Supplementary data

Supplementary data associated with this article can be found, in the online version, at <http://dx.doi.org/10.1016/j.dnarep.2017.05.001>.

#### References

- [1] A. Ciccia, S.J. Elledge, The DNA damage response: making it safe to play with knives, *Mol. Cell.* 40 (2010) 179–204.
- [2] T. Aparicio, R. Baer, J. Gautier, DNA double-strand break repair pathway choice and cancer, *DNA Repair* 19 (2014) 169–175.
- [3] J.M. Daley, P. Sung, 53BP1, BRCA1, and the choice between recombination and end joining at DNA double-strand breaks, *Mol. Cell Biol.* 34 (2014) 1380–1388.
- [4] P. Bouwman, A. Aly, J.M. Escandell, M. Pieterse, J. Bartkova, H. van der Gulden, S. Hiddingh, M. Thanasoula, A. Kulkarni, Q. Yang, B.G. Haffty, J. Tommiska,

- C. Blomqvist, R. Drapkin, D.J. Adams, H. Nevanlinna, J. Bartek, M. Tarsounas, S. Ganesan, J. Jonkers, 53BP1 loss rescues BRCA1 deficiency and is associated with triple-negative and BRCA-mutated breast cancers, *Nat. Struct. Mol. Biol.* 17 (2010) 688–695.
- [5] S.F. Bunting, E. Callen, N. Wong, H.T. Chen, F. Polato, A. Gunn, A. Bothmer, N. Feldhahn, O. Fernandez-Capetillo, L. Cao, X. Xu, C.X. Deng, T. Finkel, M. Nussenzweig, J.M. Stark, A. Nussenzweig, 53BP1 inhibits homologous recombination in Brca1-deficient cells by blocking resection of DNA breaks, *Cell* 141 (2010) 243–254.
- [6] E. Callen, M. Di Virgilio, M.J. Kruhlak, M. Nieto-Soler, N. Wong, H.T. Chen, R.B. Faryabi, F. Polato, M. Santos, L.M. Starnes, D.R. Wesemann, J.E. Lee, A. Tubbs, B.P. Sleckman, J.A. Daniel, K. Ge, F.W. Alt, O. Fernandez-Capetillo, M.C. Nussenzweig, A. Nussenzweig, 53BP1 mediates productive and mutagenic DNA repair through distinct phosphoprotein interactions, *Cell* 153 (2013) 1266–1280.
- [7] J.R. Chapman, P. Barral, J.B. Vannier, V. Borel, M. Steger, A. Tomas-Loba, A.A. Sartori, I.R. Adams, F.D. Batista, S.J. Boulton, RIF1 is essential for 53BP1-dependent nonhomologous end joining and suppression of DNA double-strand break resection, *Mol. Cell.* 49 (2013) 858–871.
- [8] M. Di Virgilio, E. Callen, A. Yamane, W. Zhang, M. Jankovic, A.D. Gitlin, N. Feldhahn, W. Resch, T.Y. Oliveira, B.T. Chait, A. Nussenzweig, R. Casellas, D.F. Robbiani, M.C. Nussenzweig, RIF1 prevents resection of DNA breaks and promotes immunoglobulin class switching, *Science* 339 (2013) 711–715.
- [9] C. Escribano-Diaz, A. Orthwein, A. Fradet-Turcotte, M. Xing, J.T. Young, J. Tkac, M.A. Cook, A.P. Rosebrock, M. Munro, M.D. Canny, D. Xu, D. Durocher, A cell cycle-dependent regulatory circuit composed of 53BP1-RIF1 and BRCA1-CtIP controls DNA repair pathway choice, *Mol. Cell.* 49 (2013) 872–883.
- [10] L. Feng, K.W. Fong, J. Wang, W. Wang, J. Chen, RIF1 counteracts BRCA1-mediated end resection during DNA repair, *J. Biol. Chem.* 288 (2013) 11135–11143.
- [11] M. Zimmermann, F. Lotterberger, S.B. Buonomo, A. Sfeir, T. de Lange, 53BP1 regulates DSB repair using RIF1 to control 5' end resection, *Science* 339 (2013) 700–704.
- [12] D. Xu, P. Muniandy, E. Leo, J. Yin, S. Thangavel, X. Shen, M. Li, K. Agama, R. Guo, D. Fox 3rd, A.R. Meetei, L. Wilson, H. Nguyen, N.P. Weng, S.J. Brill, L. Li, A. Vindigni, Y. Pommier, M. Seidman, W. Wang, RIF1 provides a new DNA-binding interface for the Bloom syndrome complex to maintain normal replication, *EMBO J.* 29 (2010) 3140–3155.
- [13] E. Sreesankar, R. Senthilkumar, V. Bharathi, R.K. Mishra, K. Mishra, Functional diversification of yeast telomere associated protein, RIF1, in higher eukaryotes, *BMC Genomics* 13 (2012) 255.
- [14] J. Wang, A. Aroumougame, M. Lobrich, Y. Li, D. Chen, J. Chen, Z. Gong, PTIP associates with Artemis to dictate DNA repair pathway choice, *Genes. Dev.* 28 (2014) 2693–2698.
- [15] M. Dutertre, S. Lambert, A. Carreira, M. Amor-Gueret, S. Vagner, DNA damage: RNA-binding proteins protect from near and far, *Trends Biochem. Sci.* 39 (2014) 141–149.
- [16] R. Ohsawa, J.H. Seol, J.K. Tyler, At the intersection of non-coding transcription DNA repair, chromatin structure, and cellular senescence, *Front. Genet.* 4 (2013) 136.
- [17] C. Naro, P. Bielli, V. Pagliarini, C. Sette, The interplay between DNA damage response and RNA processing: the unexpected role of splicing factors as gatekeepers of genome stability, *Front. Genet.* 6 (2015) 142.
- [18] L. Li, E.A. Monckton, R. Godbout, A role for DEAD box 1 at DNA double-strand breaks, *Mol. Cell Biol.* 28 (2008) 6413–6425.
- [19] L. Li, D.R. Germain, H.Y. Poon, M.R. Hildebrandt, E.A. Monckton, D. McDonald, M.J. Hendzel, R. Godbout, DEAD box 1 facilitates removal of RNA and homologous recombination at DNA double-strand breaks, *Mol. Cell Biol.* 36 (2016) 2794–2810.
- [20] C. Han, Y. Liu, G. Wan, H.J. Choi, L. Zhao, C. Ivan, X. He, A.K. Sood, X. Zhang, X. Lu, The RNA-binding protein DDX1 promotes primary microRNA maturation and inhibits ovarian tumor progression, *Cell Rep.* 8 (2014) 1447–1460.
- [21] R. Godbout, J. Squire, Amplification of a DEAD box protein gene in retinoblastoma cell lines, *Proc. Natl. Acad. Sci. U. S. A.* 90 (1993) 7578–7582.
- [22] R. Godbout, L. Li, R.Z. Liu, K. Roy, Role of DEAD Box 1 in retinoblastoma and neuroblastoma, *Future Oncol.* 3 (2007) 575–587.
- [23] D.R. Germain, K. Graham, D.D. Glubrecht, J.C. Hugh, J.R. Mackey, R. Godbout, DEAD Box 1: a novel and independent prognostic marker for early recurrence in breast cancer, *Breast Cancer Res. Treat.* 127 (2011) 53–63.
- [24] M.R. Hildebrandt, D.R. Germain, E.A. Monckton, M. Brun, R. Godbout, Ddx1 knockout results in transgenerational wild-type lethality in mice, *Sci. Rep.* 5 (2015) 9829.
- [25] D.R. Germain, L. Li, M.R. Hildebrandt, A.J. Simmonds, S.C. Hughes, R. Godbout, Loss of the *Drosophila* melanogaster DEAD box protein Ddx1 leads to reduced size and aberrant gametogenesis, *Dev. Biol.* 407 (2015) 232–245.
- [26] Y. Kanai, N. Dohmae, N. Hirokawa, Kinesin transports RNA: isolation and characterization of an RNA-transporting granule, *Neuron* 43 (2004) 513–525.
- [27] L.C. Miller, V. Blandford, R. McAdam, M.R. Sanchez-Carbente, F. Badaeux, L. DesGroseillers, W.S. Sossin, Combinations of DEAD box proteins distinguish distinct types of RNA: protein complexes in neurons, *Mol. Cell. Neurosci.* 40 (2009) 485–495.
- [28] Z. Zhang, T. Kim, M. Bao, V. Facchinetti, S.Y. Jung, A.A. Ghaffari, J. Qin, G. Cheng, Y.J. Liu, DDX1, DDX21, and DHX36 helicases form a complex with the adaptor molecule TRIF to sense dsRNA in dendritic cells, *Immunity* 34 (2011) 866–878.
- [29] C.H. Wu, P.J. Chen, S.H. Yeh, Nucleocapsid phosphorylation and RNA helicase DDX1 recruitment enables coronavirus transition from discontinuous to continuous transcription, *Cell Host. Microb.* 16 (2014) 462–472.
- [30] L. Xu, S. Khadijah, S. Fang, L. Wang, F.P. Tay, D.X. Liu, The cellular RNA helicase

- DDX1 interacts with coronavirus nonstructural protein 14 and enhances viral replication, *J. Virol.* 84 (2010) 8571–8583.
- [31] J. Popow, J. Jurkin, A. Schleiffer, J. Martinez, Analysis of orthologous groups reveals archease and DDX1 as tRNA splicing factors, *Nature* 511 (2014) 104–107.
- [32] G. Candiano, M. Bruschi, L. Musante, L. Santucci, G.M. Ghiggeri, B. Carnemolla, P. Orecchia, L. Zardi, P.G. Righetti, Blue silver: a very sensitive colloidal Coomassie G-250 staining for proteome analysis, *Electrophoresis* 25 (2004) 1327–1333.
- [33] D.M. Creasy, J.S. Cottrell, Error tolerant searching of uninterpreted tandem mass spectrometry data, *Proteomics* 2 (2002) 1426–1434.
- [34] S. Bleoo, X. Sun, M.J. Hendzel, J.M. Rowe, M. Packer, R. Godbout, Association of human DEAD box protein DDX1 with a cleavage stimulation factor involved in 3'-end processing of pre-mRNA, *Mol. Biol. Cell* 12 (2001) 3046–3059.
- [35] L. Li, K. Roy, S. Katyal, X. Sun, S. Bleoo, R. Godbout, Dynamic nature of cleavage bodies and their spatial relationship to DDX1 bodies, Cajal bodies, and gems, *Mol. Biol. Cell* 17 (2006) 1126–1140.
- [36] B. Xia, Q. Sheng, K. Nakanishi, A. Ohashi, J. Wu, N. Christ, X. Liu, M. Jasin, F.J. Couch, D.M. Livingston, Control of BRCA2 cellular and clinical functions by a nuclear partner, PALB2, *Mol. Cell* 22 (2006) 719–729.
- [37] A. Gunn, N. Bennardo, A. Cheng, J.M. Stark, Correct end use during end joining of multiple chromosomal double strand breaks is influenced by repair protein RAD50, DNA-dependent protein kinase DNA-PKcs, and transcription context, *J. Biol. Chem.* 286 (2011) 42470–42482.
- [38] J. Silverman, H. Takai, S.B. Buonomo, F. Eisenhaber, T. de Lange, Human Rif1 ortholog of a yeast telomeric protein, is regulated by ATM and 53BP1 and functions in the S-phase checkpoint, *Genes. Dev.* 18 (2004) 2108–2119.
- [39] M. Hayano, Y. Kanoh, S. Matsumoto, C. Renard-Guillet, K. Shirahige, H. Masai, Rif1 is a global regulator of timing of replication origin firing in fission yeast, *Genes. Dev.* 26 (2012) 137–150.
- [40] S. Yamazaki, A. Ishii, Y. Kanoh, M. Oda, Y. Nishito, H. Masai, Rif1 regulates the replication timing domains on the human genome, *EMBO J.* 31 (2012) 3667–3677.
- [41] D. Cornacchia, V. Dileep, J.P. Quivy, R. Foti, F. Tili, R. Santarella-Mellwig, C. Antony, G. Almouzni, D.M. Gilbert, S.B. Buonomo, Mouse Rif1 is a key regulator of the replication-timing programme in mammalian cells, *EMBO J.* 31 (2012) 3678–3690.
- [42] S.A. Kunde, L. Musante, A. Grimme, U. Fischer, E. Muller, E.E. Wanker, V.M. Kalscheuer, The X-chromosome-linked intellectual disability protein PQBP1 is a component of neuronal RNA granules and regulates the appearance of stress granules, *Hum. Mol. Genet.* 20 (2011) 4916–4931.
- [43] F. Pryde, S. Khalili, K. Robertson, J. Selfridge, A.M. Ritchie, D.W. Melton, D. Jullien, Y. Adachi, 53BP1 exchanges slowly at the sites of DNA damage and appears to require RNA for its association with chromatin, *J. Cell Sci.* 118 (2005) 2043–2055.
- [44] S. Francia, F. Michelini, A. Saxena, D. Tang, M. de Hoon, V. Anelli, M. Mione, P. Carninci, F. d'Adda di Fagnana, Site-specific DICER and DROSHA RNA products control the DNA-damage response, *Nature* 488 (2012) 231–235.
- [45] T. Conrad, A.S. Albrecht, V.R. de Melo Costa, S. Sauer, D. Meierhofer, U.A. Orom, Serial interactome capture of the human cell nucleus, *Nat. Commun.* 7 (2016) 11212.
- [46] M. Schwartz, E. Zlotorynski, M. Goldberg, E. Ozeri, A. Rahat, C. le Sage, B.P. Chen, D.J. Chen, R. Agami, B. Kerem, Homologous recombination and nonhomologous end-joining repair pathways regulate fragile site stability, *Genes. Dev.* 19 (2005) 2715–2726.
- [47] S.B. Buonomo, Y. Wu, D. Ferguson, T. de Lange, Mammalian Rif1 contributes to replication stress survival and homology-directed repair, *J. Cell Biol.* 187 (2009) 385–398.
- [48] S. Gravel, J.R. Chapman, C. Magill, S.P. Jackson, DNA helicases Sgs1 and BLM promote DNA double-strand break resection, *Genes. Dev.* 22 (2008) 2767–2772.
- [49] A.V. Nimonkar, J. Genschel, E. Kinoshita, P. Polaczek, J.L. Campbell, C. Wyman, P. Modrich, S.C. Kowalczykowski, BLM-DNA2-RPA-MRN and EXO1-BLM-RPA-MRN constitute two DNA end resection machineries for human DNA break repair, *Genes. Dev.* 25 (2011) 350–362.
- [50] A.V. Nimonkar, A.Z. Ozsoy, J. Genschel, P. Modrich, S.C. Kowalczykowski, Human exonuclease 1 and BLM helicase interact to resect DNA and initiate DNA repair, *Proc. Natl. Acad. Sci. U. S. A.* 105 (2008) 16906–16911.
- [51] J.R. Chapman, M.R. Taylor, S.J. Boulton, Playing the end game: DNA double-strand break repair pathway choice, *Mol. Cell.* 47 (2012) 497–510.
- [52] L.S. Symington, J. Gautier, Double-strand break end resection and repair pathway choice, *Annu. Rev. Genet.* 45 (2011) 247–271.
- [53] D. Cortez, Y. Wang, J. Qin, S.J. Elledge, Requirement of ATM-dependent phosphorylation of brca1 in the DNA damage response to double-strand breaks, *Science* 286 (1999) 1162–1166.
- [54] I. Rappold, K. Iwabuchi, T. Date, J. Chen, Tumor suppressor p53 binding protein 1 (53BP1) is involved in DNA damage-signaling pathways, *J. Cell Biol.* 153 (2001) 613–620.
- [55] G. Ira, A. Nussenzweig, A new Riff: Rif1 eats its cake and has it too, *EMBO Rep.* 15 (2014) 622–624.
- [56] M. Martina, D. Bonetti, M. Villa, G. Lucchini, M.P. Longhese, *Saccharomyces cerevisiae* Rif1 cooperates with MRX-Sae2 in promoting DNA-end resection, *EMBO Rep.* 15 (2014) 695–704.
- [57] Y. Hu, R. Scully, B. Sobhian, A. Xie, E. Shestakova, D.M. Livingston, RAP80-directed tuning of BRCA1 homologous recombination function at ionizing radiation-induced nuclear foci, *Genes. Dev.* 25 (2011) 685–700.
- [58] C. Ohle, R. Tesorero, G. Schermann, N. Dobrev, I. Sinning, T. Fischer, Transient RNA-DNA hybrids are required for efficient double-strand break repair, *Cell* 167 (2016) 1001–1013 (e1007).
- [59] H. Wang, A. Zhao, L. Chen, X. Zhong, J. Liao, M. Gao, M. Cai, D.H. Lee, J. Li, D. Chowdhury, Y.G. Yang, G.P. Pfeifer, Y. Yen, X. Xu, Human RIF1 encodes an anti-apoptotic factor required for DNA repair, *Carcinogenesis* 30 (2009) 1314–1319.
- [60] A. Chakraborty, N. Tapryal, T. Venkova, N. Horikoshi, R.K. Pandita, A.H. Sarker, P.S. Sarkar, T.K. Pandita, T.K. Hazra, Classical non-homologous end-joining pathway utilizes nascent RNA for error-free double-strand break repair of transcribed genes, *Nat. Commun.* 7 (2016) 13049.
- [61] L. Xu, E.H. Blackburn, Human Rif1 protein binds aberrant telomeres and aligns along anaphase midzone microtubules, *J. Cell Biol.* 167 (2004) 819–830.
- [62] L. Wu, I.D. Hickson, The Bloom's syndrome helicase suppresses crossing over during homologous recombination, *Nature* 426 (2003) 870–874.
- [63] S. Raynard, W. Bussen, P. Sung, A double Holliday junction dissolvasome comprising BLM, topoisomerase IIIalpha, and BLAP75, *J. Biol. Chem.* 281 (2006) 13861–13864.
- [64] R.M. Brosh Jr., J.L. Li, M.K. Kenny, J.K. Karow, M.P. Cooper, R.P. Kurekattil, I.D. Hickson, V.A. Bohr, Replication protein A physically interacts with the Bloom's syndrome protein and stimulates its helicase activity, *J. Biol. Chem.* 275 (2000) 23500–23508.
- [65] X. Xue, S. Raynard, V. Busygina, A.K. Singh, P. Sung, Role of replication protein A in double holliday junction dissolution mediated by the BLM-Topo IIIalpha-RMI1-RMI2 protein complex, *J. Biol. Chem.* 288 (2013) 14221–14227.